Published in final edited form as:
Eur J Neurosci. 2013 March ; 37(6): 860–875. doi:10.1111/ejn.12104.

Putative Excitatory and Putative Inhibitory Inputs Localize to Different Dendritic Domains in a Drosophila Flight Motoneuron

Claudia Kuehn[1] and **Carsten Duch**[1,2]

[1]School of Life Sciences, Arizona State University, Tempe, 85287, AZ

[2]Institute of Neurobiology, Johannes Gutenberg University of Mainz, 55099 Mainz, Germany

Abstract

Input-output computations of individual neurons may be affected by the three-dimensional structure of their dendrites and by the targeting of input synapses to specific parts of their dendrites. However, only few examples exist where dendritic architecture can be related to behaviorally relevant computations of a neuron. By combining genetic, immunohistochemical, and confocal laser scanning methods this study estimates the location of the spike initiating zone and the dendritic distribution patterns of putative synaptic inputs on an individually identified Drosophila flight motorneuron, MN5. MN5 is a monopolar neuron with more than 4000 dendritic branches. The site of spike initiation was estimated by mapping sodium channel immunolabel onto geometric reconstructions of MN5. Maps of putative excitatory cholinergic and of putative inhibitory GABAergic inputs on MN5 dendrites were created by charting tagged Dα7 nicotinic acetylcholine receptors and Rdl $GABA_A$ receptors onto MN5 dendritic surface reconstructions. Although these methods provided only an estimate of putative input synapse distributions, the data indicated that inhibitory and excitatory synapses were targeted preferentially to different dendritic domains of MN5, and thus, computed mostly separately. Most putative inhibitory inputs were close to spike initiation, which was consistent with sharp inhibition, as predicted previously based on recordings of motoneuron firing patterns during flight. By contrast, highest densities of putative excitatory inputs at more distant dendritic regions were consistent with the prediction that in response to different power demands during flight, tonic excitatory drive to flight motoneuron dendrites must be smoothly translated into different tonic firing frequencies.

Keywords

motoneuron; dendrite; flight; insect

Introduction

Brain function depends on the correct synaptic connections within neural networks. However, the individual network components, single neurons, may also carry out relevant computations of synaptic input. Input-output computations in neurons are affected by dendritic geometry and the sub-dendritic distribution of input synapses (Koch & Segev, 2000; Haeusser & Mel, 2003; London & Haeusser, 2005). Therefore, one challenge toward understanding single neuron function is to determine whether different types of synaptic inputs are targeted to specific dendritic domains, and whether this might play a role for behaviorally relevant computations.

Please send all correspondence to C. Duch at the above address., Tel: 001 480 7279422, Fax: 001 480 7279440, carsten.duch@asu.edu.

One of the best studied classes of neurons, pyramidal neurons, exhibit distinct basal and apical dendrite morphologies, and different dendritic domains receive inputs from distinct classes of neurons (Ishizuka et al., 1990; Li et al., 1994; Di Cristo et al., 2004; Somogyi et al. 1998; Stricker et al. 1996), which in turn seems crucial for temporal input integration (Pouille & Scanziani, 2001). However, the stunning complexity of cortical networks makes an assessment of the behavioral consequences of pyramidal cell input-output computation as resulting from sub-dendritic synapse and ion channel distributions difficult (Katz et al., 2009).

This study aims to test whether domain specific targeting of different types of synaptic inputs occurs also in an individually identified *Drosophila* flight motoneuron, MN5, for which the firing patterns during behavior are well described. This is intended as a first step toward relating sub-dendritic synapse targeting to behavioral function.

Drosophila flight is generated by 24 flight muscle fibers, each of which is innervated by one motoneuron only. Flight is powered by specialized, stretch-activated, asynchronous flight muscles, where motoneuron action potentials are not synchronized with muscle contractions (Machin & Pringle, 1959). Instead, during flight the motoneurons fire single action potentials at tonic frequencies of 6 to 20 Hz, which equals to every 10^{th} to 20^{th} wingbeat. Neuromuscular transmission may elevate the intramuscular calcium concentration to prime asynchronous flight muscle for stretch activation by contractions of antagonists (Dickinson & Tu, 1997). Wing depression is powered by the dorsal longitudinal flight muscle (DLM) consisting of six muscle fibers. Fibers 1 to 4 are innervated by MNs1-4, and MN5 innervates fibers 5 and 6 (Ikeda & Koenig, 1988; Duch et al., 2000). Simultaneous recordings of MN1-5 during restrained flight of intact flies have shown that MN1-5 fire tonically at similar frequencies but never in synchrony (Koenig & Ikeda, 1980a; b; Levine & Wyman, 1973; Harcombe & Wyman, 1977). Motoneuron tonic firing rates change in response to different power demands (Gordon & Dickinson, 2006). It has been hypothesized that common excitatory drive to MN1-5 is translated into tonic, slowly adjustable firing frequencies, and that inhibitory network connections prohibit simultaneous MN1-5 firing (Harcombe & Wyman, 1977).

In this study maps of putative GABAergic and cholinergic inputs through MN5 were estimated by localizing tagged and immunolabeled $GABA_A$ receptors (Rdl) and nAChRs (Dα7 subunit) on MN5 dendrite reconstructions. Targeting of putative excitatory and inhibitory inputs to complementary dendritic domains is discussed in the context of previously described MN5 firing patterns during flight.

Methods

Animals

Drosophila melanogaster strains were kept on a standard cornmeal medium at 25°C (12/12 light/dark cycle). For experiments female adult flies were used 1-3 days after eclosion. The binary GAL4-UAS expression system (Brand and Perrimon, 1993; Duffy, 2002) was utilized to express tagged ionotropic receptors, cloned to UAS elements, under the control of three recombinant motoneuron driver lines C380-GAL4, D42-GAL4 and P103.3-GAL4, respectively. All three GAL4 drivers express in a subset of motoneurons including MN5 (Yeh et al., 1995; Sanyal *et al.*, 2003; 2009; Consoulas *et al.*, 2002) and in some unidentified interneurons. To drive expression of tagged receptors in MN5, virgins females homozygous for the yeast transcription factor GAL4 expressed in motoneurons (C380-GAL4, D42-GAL4, P103.3-GAL4) were crossed with male flies that were homozygous for UAS-tagged receptor constructs. Unwanted expression of GAL4 in cholinergic interneurons was prevented by co-expression of GAL80, a suppressor for GAL4 activity, under the control of

the Cha promoter (choline-acetyl transferase) that expresses in all cholinergic neurons. The recombinant C380-GAL4, Cha-GAL80 and D42-GAL4, Cha-GAL80 were received from Dr. S. Sanyal (Emory University, Atlanta, GA) and we recombined Cha-GAL80 into P103.3-GAL4 (obtained from Dr. Consoulas, Athens, Greece). Transgenic flies carrying the UAS-Dα7-GFP construct to express GFP-tagged Dα7 subunits of the nicotinic acetylcholine receptor (nAChR, Raghu et al., 2007) were obtained from Dr. S. Sigrist (Free University of Berlin, Germany). Transgenic flies carrying the UAS-HA-tagged Rdl-$GABA_A$ receptor subunit (Raghu et al., 2009) were obtained from Dr. A. Prokop (University of Manchester, U.K.).

Intracellular labeling of the flight motoneuron, MN5

Intracellular staining of MN5 was conducted with neurobiotin as described previously (Duch et al. 2008). Briefly, animals were dissected dorsal side up in a silicone elastomer (Sylgard)-coated Petri dish. After removal of the gut and the esophagus, the ventral nerve cord was exposed. The Petri dish was mounted onto a Zeiss fluorescence microscope, and the recording chamber was superfused with standard solution composed of the following (in mM): 128 NaCl, 2 KCl, 1.8 CaCl2, 4 MgCl2, 5 HEPES, and 35.5 sucrose, pH was adjusted with 1 M NaOH to 7.2, osmolality was 295 mosmol/kg, adjusted with sucrose. For intracellular labeling of MN5, thin-walled glass microelectrodes (75-95 MΩ tip resistance) were filled with a mixture of 7% Neurobiotin (Linaris GmbH, Wertheim-Bettingen, Germany) and rhodamin-dextran (Invitrogen, Carlsbad, CA) in 2 M potassium acetate. An air bubble between the dye-filled tip and the shaft filled with 2 M potassium acetate prevented dye dilution. Following intracellular penetration of MN5, the dyes were injected iontophoretically by a constant depolarizing current of 0.5 nA for 10-12 min. Following electrode removal the ganglia where fixed in 4% paraformaldehyde in phosphate-buffer solution (PBS, 0.1M) for 1 h at room temperature. Ganglia were washed in PBS (0.1M) six times for 15 min each and four times in PBS-tritonX (0.5% triton in 0.1 M PBS). This was followed by overnight incubation with Cy5-streptavidin (Invitrogen, Karlsruhe, Germany; 1:750) in PBS-tritonX (0.3% triton in 0.1 M PBS) at 4°C. This was followed by 6 washes in PBS (0.1 M), dehydration in an ethanol series (see preceding text), 5-min treatment in a 1:1 mixture of pure ethanol and methyl salicylate and clearing and mounting in methyl salicylate.

Double labels with tagged receptors were conducted by combining immunostaining protocols for GFP or HA (see below) with intracellular neurobiotin (Vector Laboratories) staining. MN5 was filled, fixed, and incubated with different primary antibodies (see below). Incubation and washing was conducted as described above, and secondary antibodies (1:500 in PBS) were incubated simultaneously with Cy5-streptavidin (1:1000 in PBS, Invitrogen) overnight at 4°C. For confocal microscopy preparations were dehydrated in an ascending ethanol series (50, 70, 90, 2x 100% for 15 minutes each), cleared in a 1:1 mixture of 100% ethanol and methylsalicylate for 10 minutes, and mounted in pure methylsalicylate.

Geometric single neuron reconstructions and mapping of second labels onto reconstructed neuronal surfaces

Three-dimensional geometric reconstructions of the central arborizations of the identified Drosophila motoneuron, MN5, were conducted with custom plug-ins for Amira 4.1 (Mercury), which have been described in detail elsewhere (Schmitt et al., 2004; Evers et al., 2005; Meseke et al., 2009). The distribution of tagged receptors was mapped onto MN5 surface reconstructions as described previously (Evers et al., 2005; see also below; Meseke et al., 2009). In short, every tagged receptor that yielded positive labeling of the same voxel as an intracellularly stained dendrite was counted as a double label. All double labels were

mapped onto the dendritic surface as putative input synapses (Evers et al., 2005; Schmitt et al., 2004).

Expression of HA-tagged Rdl-$GABA_A$ receptors and GFP tagged Dα7-nAChRs to label putative excitatory cholinergic and inhibitory GABAergic inputs to the flight motoneuron, MN5

MN5 contains a complex dendritic arbor comprising more than 6500 micrometers of total length and more than 4000 branches. Metric and topological features as well as sub-domains of this dendritic arbor are well preserved from animal to animal (Vonhoff & Duch, 2010). This study tested how excitatory and inhibitory input synapses were distributed through MN5 dendrites. In the insect ventral nerve cord, nicotinic acetylcholine receptors (nAChRs) mediate fast excitatory signaling at most synapses (Leech & Sattelle, 1993; Su et al., 2003), whereas $GABA_A$ receptors are predominantly used for fast inhibitory synapses. The Drosophila genome contains 10 nAChR subunits. The Dα7 subunit is homologous to vertebrate α7 receptors (Grauso et al., 2002), can form homomeric pentamers, has high permeability for calcium, and is the predominant nAChR of all neurons of the Drosophila escape circuit, including MN5 (Fayyazuddin et al., 2006). Accordingly, heterozygous Dα7 mutant animals fail to perform escape responses (Fayyazuddin et al., 2006).

In Drosophila, at least three genes may encode $GABA_A$ receptors, resistance to dieldrin (Rdl), GABA and glycine-like receptor (Gdr), and ligand gated chloride channel homolog (Lcch3). Rdl is the best characterized and abundantly expressed in the Drosophila brain (Ffrench-Constant et al.,1990; 1993; Harrison et al., 1996; Liu et al., 2007, Agosto et al., 2008) and ventral nerve cord (this study), and localizes to central neuron dendrites (Raghu et al., 2007).

MN5 and a subset of other neurons can be labeled by targeted expression of GFP under the control of motoneuron-specific GAL4 drivers, such as C380 (Fig. 1A, green channel), P103.3, and D42 (see above). Double labeling with an antibody against Dα7nAChRs confirmed previous work by Fayyazuddin et al. (2006) that MN5 and other neurons of the Drosophila escape circuitry abundantly express Dα7nAChR (Figs. 1A, B, magenta). As previously described (Fayyazuddin et al., 2006), immunostaining for the Dα7 receptor revealed punctuated labeling with the highest density in the neuropil region containing the dendrites of flight motoneurons, including MN5 (Fig. 1B, see dotted white oval). However, positive immunolabel for Dα7 was also found in other regions (e.g. white arrow in Fig. 1B). To restrict Dα7-GFP label to a sub-set of neurons, including MN5, UAS-Dα7-GFP was expressed under the control of P103.3-GAL4 (Consoulas et al., 2002). Co-labeling MN5 by intracellular dye filling revealed that expression of GFP-tagged Dα7nAChR under the control of P103.3-GAL4 yielded punctuated expression in neuropil regions around MN5 dendrites (Fig. 1C). All Dα7-GFP puncta that co-localized with dendrites of MN5 were mapped onto MN5 dendritic surface reconstructions (for detailed method see Evers et al., 2005; 2006). A representative selective enlargement of one MN5 dendritic branch reveals GFP tagged Dα7nAChR positive label on MN5 dendrites (Figs. 1D, dendrite in green, Dα7nAChR in magenta). All Dα7 positive puncta that were in direct contact to MN5 dendritic surface were counted as a putative synaptic contact (Fig. 1D, white arrows). However, optical resolution of confocal microscopy with a 1.2 NA 40x oil immersion lens ($0.12 \times 0.12 \times 0.3$ μm) can yield only an estimate of putative synaptic contacts. This method yields false positives whenever GFP-tagged Dα7 receptors are located on processes of other neurons which are closer than 0.3 μm to MN5 dendrites. In addition, not all Dα7-GFP positive puncta may reflect a postsynapse, which can add more false positives (Hohensee et al., 2008). Therefore, all Dα7-GFP positive puncta mapped onto MN5 dendritic surface reconstructions were accepted as a putative cholinergic inputs only if a NC82 positive punctum was present within 0.3 μm from the putative postsynaptic site (Fig. 1E). NC82

labels the Bruchpilot (Brp) scaffolding protein located in all presynaptic active zones in the neuropil (Wagh et al. 2006). This limited postsynaptic puncta counts to locations that were in direct contact with a presynaptic terminal (Figs. 1D, E, white arrows).

A similar approach was conducted for mapping of putative inhibitory GABAergic contacts. First, immunocytochemistry for native Rdl $GABA_A$ receptors revealed punctuated label throughout the ventral nerve cord, including the mesothoracic motor neuropil where MN5 is located (Fig. 1F, magenta channel). High densities of punctuated anti-Rdl receptor immunostaining were detected in the mesothoracic motor neuropil that contains also the dendrites of MN5 (Fig. 1G, white circle). To restrict Rdl $GABA_A$ receptor detection to few neurons, including MN5, HA-tagged Rdl receptors were expressed under the control of three different motoneuron GAL-driver lines (P103.3-GAL4, Dd42-GAL4, and C380-GAL4, each with Cha-GAL80 on the third chromosome). Expression in all three driver lines yielded punctuated expression through MN5 dendrites, and visual inspection of confocal images showed qualitatively similar distribution patterns through MN5 dendrites (not shown). Pairing intracellular stainings of MN5 with Rdl-HA immunocytochemistry allowed mapping of Rdl puncta onto MN5 dendrites (Fig. 1H). Close-ups of representative MN5 dendritic branches revealed co-localization of Rdl-HA positive puncta and MN5 dendrites (Figs. 1I and 1J, see arrows). Such direct contacts, within the resolution limits of confocal microscopy, were considered putative GABAergic inputs to MN5 dendrites and mapped onto MN5 dendritic surface reconstructions (Evers et al., 2005; Schmitt et al., 2004). Rdl-HA immunocytochemistry was not paired with NC82 immunocytochemistry because we observed cross-reactivity between both primary antibodies, one of which was made in mouse (NC82) and one of which was made in rat (anti-HA). Expression of Rdl-HA in central Drosophila neurons has previously been used successfully to determine the sub-neuronal localization of $GABA_A$ receptors (Raghu et al., 2007).

Although all three GAL4 drivers (C380, P103.3, D42,) were tested, all quantification for the localization of Dα7-GFP was carried out following expression under the control of P103.3, whereas all quantification of the localization of Rdl-HA was carried out following expression under the control of C380. This choice was based on data analysis. To determine the threshold for accepting a voxel as immunopositive, the staining intensities of all voxels within a given confocal imaging channel (immnuolabeled HA, NC82, or Dα7) were plotted as frequency distribution. Threshold was defined at the brightest 10% of all voxels (for details see Meseke et al., 2009). For Dα7 contrast turned out to be sharpest when the GFP tagged transgene was expressed under the control of P103.3-GAL4, whereas for Rdl-HA the sharpest contrast was observed following expression under the control of C380-GAL4. Although the overall density of putative GABAergic of putative cholinergic was affected by changing threshold values, the distribution patterns through MN5 dendrites were qualitatively independent of varying threshold within a reasonable range. MN5 dendritic morphology shows no statistically significant differences between P103.3 and C380 control animals, neither with regard to metric measures like total dendritic length or branch number nor with regard to topological measures like dendritic surface or dendritic length distribution in Sholl spheres or with respect to branch order (Vonhoff & Duch, 2010). Therefore, potential differences in receptor localization are not caused by differences in dendritic morphology in these different GAL4 driver strains.

Immunocytochemistry

Dα7-GFP was detected with a primary anti-GFP antibody (Invitrogen, rabbit anti-GFP, A11122). Rdl-HA was detected with a primary anti-HA antibody (Roche, rat anti-GFP, 11867423001, clone 3F-10). The Dα7 nAChR antibody was a kind gift of Dr. H Bellen, BCM, Houston Texas), and antibody specificity has previously been proven by absence of immunolabel in null mutants (Fayyazuddin et al., 2006). The anti-RDL $GABA_A$ receptor

antibody was a kind gift of Dr. Naessel (Stockholm, Sweden), and its specificity has been characterized by Western blotting, immunocytochemistry, pre-absorption with immunization peptide, and by tests with pre-immune serum (Enell et al., 2007). For RDL immunocytochemistry, tissue was fixed in 2% formalin and 1% SMB for 30 minutes, washed for 2 hours in PBS-tritonX (0.5%). Primary RDL antibody was applied for 24 hours at 4° C at a concentration of 1:10000 in PBS-tritonX (0.5%) and 2% normal goat serum. For Dα7 nAChR immunocytochemistry tissue was fixed for 20 minutes in 4 % paraformaldehyde, washed in PBS overnight, and washed for 3 hours in PBS-tritonX (0.5%). Primary Dα7 nAChR antibody was applied for 48 hours at 4° C at a concentration of 1:2000 in PBS-tritonX (0.3%) and 3% bovine albumin serum.

For the labeling of sodium channels, a polyclonal antibody (Chemicon International, AB5210) against a purified peptide (SP19 of the alpha subunit; amino acids 1500-1518) of rat type I VGSC (accession no. P04774) was applied at a dilution of 1:200. Specificity of the SP19 antibody for the insect sodium channel has been demonstrated previously (French et al., 1993; Amat et al. 1998; Boerner et al., 2006) and was confirmed for *Drosophila melanogaster* in this study by Western blotting. Secondary antibodies were used as previously described (Boerner & Duch, 2010).

Western blotting

For Western blot analysis of embryonic tissue, embryos (100 per lane) were homogenized in 100μl sample buffer (7 mL 4x Tris-Cl/SDS, pH 6.8; 3.6 mL glycerol; 1 g SDS; 0.93 g DTT; 1 mg bromophenol blue; add ddH_2O to a volume of 10ml) using a sterile plastic pistil. Samples were boiled immediately in a water bath for 3 minutes and then frozen at −20°C until needed. Genotypes were Canton^S as control strain and para Df(1) D34/Fm7 (generously provided by R. Baines, Manchester). The Df(1)D34 mutant is reportedly a functional null (Baines and Bate, 1998; see http://flybase.org/reports/FBab0000366.html). The chromosomal deletion (14C6-14D1) overlaps with part of the para gene (14D1 to 16A2), and homozygous mutant flies are late embryonic lethal (Broadie & Bate, 1993; Baines & Bate, 1998; Mee et al., 2004). We collected 100 mutant (Df(1)D34) and 100 control (Canton^S) embryos at 18 hAEL (late embryonic stage 16, early stage 17). We used a glycin/polyacrylamide gel (30 ml volume) consisting of two phases (5% SDS-PAGE running gel (~30 mL), pH 8.8 consisting of 5 mL 30% bis-acrylamide (Bio-Rad), 7.5 mL 4x TRIS/SDS, pH 8.8, 17.5 mL dd H_2O, 150 μL 10% ammonium persulfate (biorad), 10 μL TEMED (Bio-Rad); Stacking gel 4% (~10 mL), pH 6.8, 6.1 mL dd H_2O, 1.34 mL 30% bis-acrylamide, 2.5 mL 4x TRIS/SDS, pH 6.8, 50 μL 10% ammoniumpersulfate, 2.5 μL TEMED). The running gel was coated with n-butanol to avoid exposure to oxygen and then allowed to polymerize for about one hour at room temperature. After removal of the n-butanol, the separating gel was poured. A 1.5 mm wide spacer for 15 pockets (100μl) was put into the stacking gel. Then the gel was allowed to polymerize and stored over night at 4°C. The Western was run at 15 mA for approximately 30 min to get through the stacking gel. As soon as the samples reached the running gel, current was increased to 30 mA. The gel was run for 5 hours at room temperature until the blue front reached the bottom of the gel. The separated proteins were transferred on a nitrocellulose membrane (Bio-Rad). The transfer was done overnight at 4°C at 35 V in an upright blotting chamber (Hoeffer) using 5.5 L of transfer buffer (18.2g Tris base, 86.5g glycine (Bio-Rad), 900 mL methanol (Sigma) add dd H_20 to 6L). The membrane was incubated for 2 hours in 10% dried milk powder blocking solution in TBST at room temperature to avoid unspecific binding of primary antibodies. The nitrocellulose membrane was washed in TBST (10 mL 1M Tris pH 7.5 and 30 mL 5M NaCl in 1l) for 3×20 min at room temperature.

Primary antibodies against the SP19 domain from rat voltage gated sodium channel raised in rabbit (1:400; Millipore, cat # 5210) and heat-shock protein 90 (hsp90, 1:1000; Cell

Signaling Technology, cat # 4874) were used. Hsp 90 antibody was used as protein loading control. Antibodies were prepared in TBST with 2.5% dried milk. Antibody incubation was done overnight at 4°C and followed by washing in TBST for 3×20 min at room temperature. Horseradish Peroxidase (HRP) conjugated anti rabbit antibody (Millipore, cat # AP106P) was used at a concentration of 1:5000 to detect both primary antibodies. Antibody incubation was done for two hours at room temperature. Detection of protein bands was done with Immobilon Western Chemiluminescent HRP Substrate (Millipore, cat # WBKL S00 50) for 3 min. For Western blotting with adult CNS, the same protocol was used with 10 brains per lane.

Image acquisition

All images were acquired with a 40x oil-immersion objective (NA 1.2) with a Leica SP2 confocal laser scanning microscope at a sampling density of 1,024 × 1,024 pixels and *z*-step size of 0.3 μm. Maximum optical resolution was 120 nm (x-dimension) × 120 nm (y-dimension) × 300 nm (z-dimension). Cy2 was excited with an argon laser at 488 nm and detected between 500 and 530 nm. Cy3 was excited with a Krypton laser at 568 nm and detected between 575 and 620 nm, and Cy5 was excited with a helium neon laser at 633 nm and detected between 640 and 700 nm. Cy2 and Cy5 were excited and detected simultaneously, but Cy3 was scanned separately in sequential scan mode with excitation wavelengths switching between each frame (488 nm and 633 nm simultaneously for Cy2 and Cy5, and 568 nm separately for Cy3). At the moderate laser and detector intensities needed no bleed through between any of the three channels was observed. All images were saved as tiff stacks and further processed with AMIRA 4.1.1 (Mercury Systems), Adobe Photoshop, and Adobe Illustrator (Version CS3).

Results

As many insect motoneurons, MN5 is a monopolar neuron (Fig. 2A). Its large soma is located in the mesothoracic neuromere of the ventral nerve cord (VNC), contralateral to its target muscle. MN5 dendrites comprise more than 6 mm of total length and spans large parts of the dorsal mesothoracic motor neuropil (Vonhoff & Duch, 2010). All primary dendrites and the axon arise from a primary neurite that connects to the soma (Fig. 2A). Together with four other motoneurons, MN1-4, MN5 innervates the dorsal longitudinal flight muscle (DLM, Fig. 2B), which provides the main force for wing down stroke during Drosophila flight and courtship song. The DLM is an indirect, asynchronous flight muscle, which means that MN1-5 action potentials are not phase linked to DLM contractions (Levine & Wyman, 1973; Koenig & Ikeda, 1980a; b), but instead, MN1-5 fire only every 5^{th} to 20^{th} wingbeat, presumable to fuel the DLM with intracellular calcium (Gordon & Dickinson, 2006). As is the case with most insect motoneurons, the soma does not generate action potentials but is mostly passive (Duch & Levine 2000; Duch et al., 2008; Meseke et al., 2009). Furthermore, as for most monopolar invertebrate neurons, it is not clear where the action potential is initiated. A functional evaluation of MN5 structure-function relationships requires information as to where the spike initiating zone (SIZ) is localized; i.e. the site where summed synaptic inputs cause the generation of an action potential if the membrane voltage threshold for action potential initiation is exceeded.

Estimating the location of the spike initiating zone (SIZ) by sodium channel immunocytochemistry

The putative site of action potential generation in MN5 was estimated by combining immunocytochemistry for sodium channels and intracellular fills of MN5 with high resolution confocal laser scanning microscopy and co-localization analysis (Schmitt et al., 2004; Evers et al., 2005). MN5 action potentials require TTX sensitive, voltage gated

sodium channels (VGSCs; Duch et al., 2008; Ryglewski & Duch, 2009; Ryglewski et al., 2012). Consequently, all parts of the neuron that are involved in active action potential propagation should exhibit a high density of VGSCs in the membrane. Co-localization analysis of immunolabeled proteins and geometric motoneuron reconstructions has proven useful to assess the distribution of synaptically localized proteins (Duch & Mentel, 2004; Evers et al., 2006; Meseke et al., 2009) and of immunolabeled VGSCs through motoneuron arbors (Boerner et al., 2006). We used this method to estimate the location of the spike initiating zone (SIZ) in MN5 geometric reconstructions (Figs 3, 4).

Sodium channels were detected with the polyclonal SP19 antibody (see methods). Specificity of the SP19 antibody for insect sodium channels has previously been reported (French et al. 1993; Amat et al., 1998; Boerner et al., 2006). We confirmed by Western blotting that the SP19 antibody recognizes a protein of 235 kDa in adult Drosophila brain homogenate, which is the predicted size of the Drosophila voltage gated sodium channel the paralytic (*para, DmNa*$_v$, Fig. 3E). Para is the only confirmed gene for voltage gated sodium channels in insects. In addition, we conducted Western blotting with controls and para mutant embryos. We used the Df(1)D34 mutant which is reportedly a functional null (Baines and Bate, 1998). The chromosomal deletion (14C6-14D1) overlaps with part of the para gene (14D1 to 16A2) and likely deletes the transcriptional start sites. Consequently, homozygous mutant flies are late embryonic lethal. Since para is weekly expressed at 16 hours after egg laying (AEL) and moderately at 18h AEL (Baines and Bate, 1998; flybase), there is a 2 hour time window to collect embryos for Western blotting before late embryonic lethality occurs in mutants. We collected 100 mutant (Df(1)D34) and 100 control (Canton^S) embryos at 18 hAEL and confirmed for each animal that it was late stage 16. Western blotting with the SP19 antibody revealed a prominent band at 240 kDa in control embryos (Fig. 3D, black arrow), which was absent from Df(1)D34 embryos (Fig. 3D). Hsp90 antibody was used on the same membrane as loading control and indicated similar protein amounts of both control and Df(1)D34 lanes (Fig. 3D, see bands at 90kDa). One additional band at about 120kDa was present only in embryo (Fig. 3D), but not in the adult (Fig. 3E). Taken together, these data indicate that the SP19 antibody recognized para in embryonic and adult tissue, and that no other proteins were recognized at the concentration used in adult tissue.

Sodium channel immunocytochemistry revealed prominent labeling of axon in tracts in the ventral nerve cord and in bundles running through nerves (Fig. 3A, white and magenta panels). Intracellular dye fills of MN5 via somatic recordings (Fig. 3A, green) revealed its axon arbors on the two dorsal most fibers of the DLM target muscle (Fig. 3A, green MN5 arbors on DLM5 and DLM6). Double labels revealed positive sodium channel staining in the axon of MN5 projecting in nerve II1, but not in the soma or in the proximal primary neurite (Fig. 3A, grey panel).

Selective enlargements of the axon of MN5 at different distances from the soma revealed only faint sodium channel immunopositive signal in the proximal primary neurite, but prominent sodium channel immunopositive signal along all distal parts of the primary neurite and the axon (Fig. 3B). The distances from the soma that are depicted in figure 3B are demarked along the MN5 axon in figure 3A. Quantification of the staining intensities revealed significantly higher immunolabel intensities for VGSCs at all locations along the primary neurite and the axon that were more distal than 100 microns from the soma (Fig. 3C, ANOVA with Newman Keuls post hoc test, $p \leq 0.01$). Therefore, within the limits of this method (see discussion) an even density of VGSCs was revealed along the entire peripheral axon and the distal primary neurite, but a fainter signal was observed along the primary neurite at sites where dendrites branch off (Fig. 3C, within about 100 μm from the

soma). This indicated that active action potential propagation may occur in the axon and the distal primary neurite, but not in the soma or the proximal primary neurite (Figs. 3A, B, C).

To account for possible across animal variations, this procedure was repeated in 7 animals. Figure 4A depicts a surface reconstruction of only the primary neurite of MN5 from one representative preparation. White boxes demark three regions along the primary neurite for which selective enlargements of the original stainings are shown (MN5 in green, sodium channels in magenta). Region 3 (most proximal to the soma) and region 2 (in the middle between the soma and the efferent nerve root) contained some faint and diffuse immunopositive staining for voltage gated sodium channel (Fig. 4A, middle and right lower panels, magenta). This staining was not restricted to the membrane, but evenly distributed throughout the cytosol. By contrast, region 1, taken from the distal primary neurite, showed higher intensity sodium channel immunopositive label, and most of this label appeared close to the primary neurite membrane (Fig. 4A, see asterisks in lower left panel). The MN5 primary neurite reconstruction (Fig. 4A, upper panel) was color coded for sodium channel staining intensity (see methods; Evers et al., 2005; Schmitt et al., 2004), with red depicting high levels and blue indicating low levels. This revealed a sharp border at about 100 microns distance from the soma, with low levels of sodium channels between this border and the soma, and high levels between this border and the target muscle (Figs. 3A, 4A see arrow).

The same border between low and high intensity VGSC label was found in MN5 in all 7 animals tested on the distal primary neurite at a distance of 11 ± 3 μm around the origin of the most distal posterior dendrite (blue; Figs. 4B, C; 11.25 μm and 12.1 μm). Two representative geometric reconstructions of MN5 are shown in figures 4B and C. The posterior dendrite branching off the primary neurite most distally from the soma is depicted in blue. Due to the characteristic shape of MN5 between animals (Vonhoff, Duch, 2010), these data now allow to estimate the location of the SIZ without sodium channel immunostainings. Within the limits of this method (see discussion) the site of action potential generation (SIZ) can now be estimated in MN5 across animals within a distance of about 12 micrometers in either direction along the primary neurite from the origin of this dendrite.

The distribution of putative cholinergic input synapses through MN5 dendrites

Next we tested whether putative excitatory cholinergic and putative inhibitory GABAergic inputs were targeted to specific dendritic sub-domains of MN5. In the insect ventral nerve cord, nicotinic acetylcholine receptors (nAChRs) mediate fast excitatory signaling at most synapses (Leech, Sattelle, 1993; Su et al., 2003), whereas $GABA_A$ receptors are predominantly used for fast inhibitory synapses. Of the ten Drosophila nAChR subunits, the Dα7 subunit is predominantly expressed by all neurons of the escape circuit, including MN5 (Fayyazudin et al., 2006).

A GFP-tagged Dα7 nAChR (Raghu et al., 2009) subunit was expressed under the control of P103.3-GAL4 (see methods). MN5 was stained intracellularly, and the distribution of GFP labeled receptors was mapped onto geometric reconstructions of MN5 dendritic structure (see methods, Figs. 2A, 5A, B). In addition the neuropil was counter-labeled with the active zone marker, NC82 (Wagh et al., 2006), to detect all presynaptic terminals as puncta (Wagh et al, 2006). A putative cholinergic synaptic contact was defined by two criteria (for detail see methods, Figs. 1C to E). First, GFP-tagged Dα7 label had to be within the dendritic surface reconstruction of MN5. Second, an NC82 positive active zone had to be within 300 nm of the Dα7 positive MN5 dendrite. This means that a positive putative synaptic contact was accepted only if the receptor and a presynaptic terminal where present at this dendritic location within the limitations of standard high resolution (NA=1.2) confocal laser scanning

microscopy. At this resolution voxel size was 120 nm × 120 nm × 300 nm (x, y, and z dimensions).

A projection view of an intracellular staining in an animal with Dα7-GFP expression under the control of P103.3-GAL is depicted in figure 5A (green). Mapping the co-localization of Dα7-GFP and NC82 puncta onto MN5 geometric reconstructions yielded a map of putative nicotinic contacts via Dα7 receptors onto MN5 (Fig. 5B). Visual inspection of such maps from 5 different animals showed that putative cholinergic inputs were present through most dendrites of MN5 and not exclusively limited to one specific dendritic sub-domain. However, in all animals two dendritic regions were mostly devoid of Dα7-GFP puncta. First, the most anterior dendrites which project in an arch from the SIZ to the cell body are mostly devoid of cholinergic input synapses (Fig. 5B, see white arrow 1). Second, a dendritic region proximal and anterior with respect to the SIZ was mostly devoid of Dα7-GFP puncta (Fig. 5B, see white arrow 2). All other dendritic sub-trees (as defined in Vonhoff & Duch, 2010) received putative cholinergic input synapses. However, the highest density of Dα7-GFP puncta appeared to be localized in a region proximal to the soma (Fig. 5B, see dotted oval).

One potential problem is that our motoneuron drivers express in more neurons than just MN5. Both C380-GAL4 and P103.3-GAL4 in conjunction with Cha-GAL80 express in about 20 neurons per thoracic hemisegment. Although most of these not overlap with MN5 dendrites, we can't exclude the possibility that over-expression in other neurons may have resulted in some false positives in our analysis. We judge a significant artifact unlikely, because we found qualitatively similar distributions for mapped receptors with multiple different driver lines that share partly non-overlapping expression patterns (Boerner & Duch, 2010) and also with immunolabeling of native receptors (see figure 1). However, we did not repeat our quantitative mapping analysis with multiple driver lines and labeling of native receptors.

In in each preparation tested (n=5) the surface of some dendritic sub-trees showed an up to four-fold higher density of putative cholinergic inputs than that of others. Dendritic regions with high densities of putative cholinergic inputs were similar between animals. For visualization purposes four MN5 dendrite reconstructions were color coded for putative cholinergic inputs. In total 23 dendritic sub-trees emerge from the MN5 primary neurite (Vonhoff & Duch, 2010). To calculate the proportion of putative cholinergic synapses on each sub-tree relative to all putative cholinergic synapses on the whole dendritic tree, the number of positively dendritic surface on each sub-tree was divided by the sum of the total positively scored surface throughout the dendritic tree. On average, 10 ± 2 sub-trees out of 23 contained 75 percent of all putative cholinergic synapses in each single cell (n = 5). Therefore, three quarters of all putative cholinergic inputs were targeted to less than half of all dendritic sub-trees. To visualize the position of these sub-trees within the whole dendritic tree, they were color-coded using a heat map (Figs. 5C to F). The sub-tree with the highest proportion of putative cholinergic synapses (15 percent on average) was always colored in red. All sub-trees with lower percent values received colors ranging from orange (11 %) to yellow (7%) to white (< 5 % of all cholinergic inputs). Sub-trees that were not included in the 75 percent group were colored in black. Note that colors within each sub-tree do not correlate to a continuous range of percent values but each color ranks each sub-trees within the MN5 reconstructions. The highest percentage of all putative cholinergic inputs was always present on a small dendritic sub-tree located in the center of the dendritic field (red sub-tree in Figs. 5C to F, see white arrows). The remaining 75 percent of all putative cholinergic inputs always occurred on dendritic sub-trees proximal with respect to the soma (Figs. 5C to F, dotted oval). By contrast, the sum of all dendritic sub-trees that originate

close to the putative SIZ and make up more than 50 % of all dendrites contain less than 25% of all putative cholinergic inputs (dark grey in Figs. 5C to F).

To further quantify the distribution of putative nicotinic inputs through MN5, the density of Dα7 positive puncta in MN5 dendrites was evaluated with regard to branch order (Figs. 6A, B) and with respect to the distance to the spike initiating zone (Figs. 6C, D). These parameters were evaluated because branching structure and distance from the SIZ are important parameters for the passive propagation of postsynaptic potentials. For branch order analysis the SIZ was defined as the tree origin. In all five preparations analyzed, an even distribution of putative cholinergic inputs was observed through all dendritic branch orders between 1 and 45. On average in branch orders 1 to 45 about 7 percent of the dendritic surface was scored positive for putative cholinergic inputs (Fig. 6A, black line average density, grey shade represents standard error). Branch orders higher than 45 contained a higher density of putative cholinergic inputs. Note that only few branches of these high orders exist, so that relatively few synaptic inputs to these dendrites strongly affect the density values. Therefore, putative cholinergic inputs did not seem to be restricted to specific branch orders, but on average higher branch orders may receive a higher density of putative cholinergic inputs. To account for differences in maximum branch order, branch order was normalized to the highest one in each animal before averaging (Fig. 6B). In dendrites up to the half maximum branch order about 6 % of the dendritic surface was positive for putative cholinergic inputs. These values increased to up to 10 % towards higher branch orders. Therefore, putative cholinergic inputs were not targeted preferentially to specific dendritic branch orders of MN5, but on average high branch orders received about twice the density of cholinergic inputs as compared to low branch orders. Note that 95 percent of all MN5 dendritic branches belong to branch orders 40 or lower (Vonhoff & Duch, 2010). Therefore, in more than 95 % of all dendrites of MN5 about 5 % of the dendritic surface was targeted by putative cholinergic inputs. Note also that high branch orders are not necessarily located to the most distal parts of MN5 dendrites, because many dendrites branch back towards the origin of the tree (Vonhoff & Duch, 2010).

Similarly, through all dendritic distances between 1 and 65 microns from the SIZ between 5 % and 10 % of the dendritic surface were scored positive for putative cholinergic inputs, with no significant differences between different distances (Fig. 6C, black line is average, grey shade is standard error). However, in all five preparations the most distal dendrites were devoid of cholinergic inputs (Fig. 6C). These corresponded to the characteristic dendrites branching in an arch towards the soma, which are marked by the white arrow 1 in figure 5B. To account for possible effects of inter animal variability in dendritic path length, distance was normalized to the highest value in each animal before averaging (Fig. 6D). On average, about 5 % of the dendritic surface within 30 microns of the spike initiating zone (normalized value of 0.3) was positive for putative cholinergic inputs, and about 7 to 8 % of the dendritic surface at distances between 35 and 70 microns to the SIZ received putative cholinergic inputs (Fig. 6D, normalized values 0.3 to 0.65). By contrast dendritic surface at distances larger than 75 microns to the SIZ received significantly lower values or were completely devoid of cholinergic inputs (Fig. 6D, normalized values 0.7 to 1).

In summary, putative cholinergic input synapses were not restricted to specific branch orders or distances to the SIZ, but 75 % of all putative cholinergic inputs were located on the proximal dendritic sub-trees with respect to the soma. By contrast, dendritic sub-trees that originate at the spike initiating zone, including those that project in an arch back toward the soma, were mostly devoid of putative cholinergic inputs.

To account not only for the density of putative cholinergic inputs to MN5 dendrites, but also for absolute values, we plotted all positively scored dendritic surface over normalized

branch order (Fig. 6E) and over normalized distance to the SIZ (Fig. 6F). Our 3-dimensional dendrite reconstructions are triangulated surfaces (Evers et al., 2005). Therefore, we counted surface triangles that were scored positive for putative cholinergic inputs over all branch orders. More than 50 % of all putative cholinergic inputs were located in normalized branch order 0.35 to 0.75 (Fig. 6E, see black bar), corresponding to branch orders 28 to 60. With regard to distance, more than 50 % of all putative cholinergic inputs are located between normalized distances 0.2 and 0.5, corresponding to real world distances between 25 and 65 microns from the SIZ (Fig. 6F, see black bar). For clarity the total numbers of all dendritic surface triangles are also plotted as dashed lines (Figs. 6E, F). This shows that most dendritic surface is located in the first 40 branch orders and within the first 50 microns from the SIZ (Figs. 6E, F).

The distribution of putative GABAergic input synapses through MN5 dendrites

In the insect ventral nerve cord $GABA_A$ receptors are predominantly used for fast inhibitory synapses. In *Drosophila*, Rdl is the best characterized one, is abundantly expressed in the *Drosophila* brain (Harrison et al., 1996; Liu et al., 2007, Agosto et al., 2008) and ventral nerve cord (Figs. 1F, G), and localizes to central neuron dendrites (Raghu et al., 2007).

To analyze the distribution of putative inhibitory GABAergic inputs through MN5 dendrites, a HA-tagged Rdl receptor (Rdl-HA; Sánchez-Soriano et al., 2005; Raghu et al., 2007) was expressed in MN5 under the control of C380-GAL4; Cha-GAL80 (see methods). Expression of Rdl-HA in a subset of thoracic neurons, including MN5, yielded punctuated label in the motor neuropil in in MN5 dendrites (Fig. 7A). Geometric reconstruction of MN5 dendrites with subsequent mapping of Rdl-HA label yielded maps of Rdl-HA localization through MN5 dendrites (Fig. 7B, see methods; Evers et al., 2005).

Preparations with Rdl-HA (n=5) yielded qualitatively similar distribution patterns of Rdl-receptors through MN5 dendrites as intracellular staining of MN5 paired with anti-Rdl immunolabeling (n=5) in wildtype flies (not shown). Punctuated Rdl-HA expression was detected through all dendritic sub-trees of MN5, but two dendritic regions always contained a particularly high density of Rdl-HA puncta (Fig. 7B). First, the most anterior dendrites which projected in an arch from the SIZ to the cell body of MN5 contained many Rdl-HA puncta at their distal ends (see dotted oval 1 in Fig. 7B). Second, in all preparations (n=5) the highest density of Rdl-HA puncta was localized to the roots of dendrites branching off the primary neurite close and anteriorly to the SIZ (see dotted oval 2 in Fig. 7B). These two regions of highest Rdl-HA puncta density corresponded to regions with low densities of putative cholinergic inputs (compare white arrows in Fig. 5B).

As for putative cholinergic inputs (Figs. 5C to F) we tested whether putative GABAergic inputs were targeted preferentially to specific regions of MN5. To calculate the proportion of GABAergic synapses on each sub-tree relative to all putative GABAergic synapses on the whole dendritic tree, the area of positively scored dendritic surface on each sub-tree was divided by the sum of the total positively scored surface throughout the dendritic tree. On average, 8 ± 1 out of 23 sub-trees contained 75 percent of all putative GABAergic inputs in each single cell (n = 5). Therefore, three quarters of all putative GABAergic inputs were targeted to about one third of all dendritic sub-trees. To visualize the position of these sub-trees within the whole dendritic tree, they were color-coded using a heat map (Figs. 7C to F). The sub-tree with the highest proportion of putative GABAergic synapses (20 percent on average) was always colored in red. All sub-trees with lower percent values received colors ranging from orange (16 %) to yellow (12%) to white (< 5 % of all putative GABAergic input). The dendritic sub-trees with the highest proportion of putative GABAergic inputs were always located just anterior to the SIZ (Figs. 7C to F, white arrows). In addition, in all (Figs. 7C, E, F) but one (Fig. 7D) out of 5 preparations the large dendritic sub-trees which

branched in an arch toward the soma showed intermediate high densities of putative GABAergic inputs. Therefore, regions devoid of cholinergic inputs received the highest (just anterior to the SIZ) or intermediate proportions of putative GABAergic inputs. Conversely, dendritic sub-trees in the center of the dendritic field which usually receive the highest proportionof putative cholinergic inputs (see white arrows in Figs. 5C to F) showed low densities of putative GABAergic inputs (Figs. 7C to F, see yellow arrows). Therefore, dendritic regions with highest putative GABAergic input densities were devoid of cholinergic inputs, and vice versa (Figs. 5C to F, 7C to F). However, despite this complementary targeting there was still some overlap of both putative cholinergic and putative GABAergic inputs to dendritic sub-trees located proximal to the soma.

To further quantify the distribution of putative GABAergic input synapses through MN5, the density of Rdl-HA puncta through MN5 dendrites was evaluated with regard to branch order (Figs. 8A, B) and with respect to distance to the spike initiating zone (Figs. 8C, D). As for putative cholinergic inputs (see Figs. 6A, B), putative GABAergic inputs localized to all branch orders (Figs. 8A, B). On average, in the lowest 20 branch orders the density of Rdl-HA puncta was between 10 and 15 percent, but it was below 10 percent in the branch orders 20 to 40 (Fig. 8A). Particular high densities of more that 20 percent were observed in branch orders of 60 and higher (Fig. 8A). But note that only few dendrites of such high branch orders exist in MN5, so that few positively scored puncta result in high densities in these branch orders. To account for differences in maximum branch order, branch order was normalized to the highest one in each animal. This revealed a similar tendency for a bimodal distribution with higher densities in lower branch orders, smaller densities in intermediate branch orders, and highest densities in the few dendrites of the highest 15 % of all branch orders (Fig. 8B).

Although putative GABAergic inputs were detected at all distances form the SIZ, the closest 20 microns of dendrites showed a higher density of Rdl-HA puncta than all distances between 20 and 70 microns (Fig. 8C). Highest densities were found at the few dendrites which were located at a distance of more than 70 microns from the SIZ (Fig. 8C). Note that MN5 contained only few dendrites at a distance of more than 70 microns from the SIZ. These included the sub-trees branching in an arch towards the soma (see Fig. 7B, dotted white oval 1). The region demarked with white oval 2 in figure 7B corresponded to the elevated Rdl-HA puncta density in dendrites within 30 microns from the SIZ (Fig. 8C). However, the density of putative GABAergic inputs within this region just anterior to the SIZ was much higher than the average density within the first 30 microns of the SIZ, because posterior dendrites within this distance showed considerably fewer putative GABAergic inputs. Normalization to the largest distance to the SIZ confirmed this bimodal distribution, with elevated densities of putative GABAergic inputs close to the SIZ and highest densities at the distal parts of the long dendritic sub-trees that branch back to the soma (Fig. 8D). These two hot spots of putative GABAergic input corresponded to the regions of low density of putative cholinergic inputs. Therefore, putative cholinergic and putative GABAergic inputs seemed to be distributed in a complementary manner, though all dendritic sub-trees exhibited some positive label for both neurotransmitter receptors. And finally, putative GABAergic input seemed to be preferentially targeted to dendritic regions close to the7 SIZ.

To account not only for the density of putative GABAergic inputs on MN5 dendrites, but also for absolute values, we plotted all positively scored dendritic surface over normalized branch order (Fig. 8E) and over normalized distance to the SIZ (Fig. 8F). More than 50% of all putative GABAergic inputs were localized within the first 10 to 30 percent of all branch orders (Fig. 8E), which corresponds to branch orders 8 to 24. By contrast, most cholinergic inputs were found between branch orders 45 and 60 (Fig. 6E). With regard to distance more

than 50% of all putative GABAergic inputs were detected between normalized distances 0.1 and 0.35 (Fig. 8F), corresponding roughly to real world distances between 12 and 45 microns from the SIZ (Fig. 6F). By contrast, most cholinergic inputs were localized at distances between 25 and 65 microns (Fig. 6F). This confirmed that the majority of most putative GABAergic inputs were located considerably closer to the SIZ than the majority of putative cholinergic inputs.

Expression of tagged receptors in MN5 does not affect overall dendritic length and branch number

One potential caveat in our approach is that both tagged receptor transgenes, UAS-Rdl-HA and UAS-Dα7-GFP, are biologically active, and thus might affect dendritic structure via activity dependent mechanisms. However, neither total dendritic length (Fig. 9A) nor the total number of MN5 dendritic branches (Fig. 9B) differed significantly between control animals of the C380 and of the P103.3 fly strains (C380-GAL4, Cha-GAL80 × w1118; P103.3-GAL4, Cha-GAL80 × w1118) and following overexpression of UAS-Rdl-HA under the control of C380-GAL4, or following overexpression of UAS-Dα7-GFP under the control of P103.3-GAL4 ($p > 0.3$, ANOVA). We have previously demonstrated that no significant MN5 morphological differences existed with regard to metric morphological measures like TDL and number of dendritic branches and with regard to topological measures such as dendritic length distribution over branch orders or over Sholl spheres between C380 and P103.3 animals (Vonhoff & Duch, 2010). Therefore, the observed differences in mapped nACh and $GABA_A$ receptor localization are not caused by strain specific distributions in dendritic surface.

Discussion

This study determined the putative location of the spike initiating zone (SIZ) in the Drosophila flight motoneuron, MN5, to then map the distribution of putative excitatory cholinergic and inhibitory GABAergic inputs on MN5 dendrites. The key findings, limitations of the methods, and possible functional consequences of sub-cellular synapse distributions for MN5 function during flight motor behavior are discussed below.

Mapping the location of the putative spike initiating zone by sodium channel immunocytochemistry

As for most monopolar insect neurons, the location of the SIZ in MN5 is difficult to determine. In vertebrate neurons the somatodendritic and the axonal domain are separated by the initial axonal segment (AIS). The cytoskeletal scaffold protein ankyrin G (AnkG) is the major organizing protein of the AIS, and is restricted to the AIS and nodes of ranvier in vertebrate neurons (Rasband, 2010). Loss of AnkG results is loss of sodium (Zhou et al., 1998), KNCQ potassium channels (Hedstrom, et al. 2007; Pan et al., 2006), and K_v1 potassium channels from the AIS (Van Wart et al., 2007). However, ankyrin G is first found in chordates (Hill et al., 2008), and thus invertebrate neurons lack ankyrin G mediated channel clustering at the AIS and lack nodes of ranvier. Nevertheless, specific targeting of the K_v1 potassium and fast voltage gated sodium channels (VGSCs) to the axonal domain and K_v4 potassium channels to the somatodendritic domain has been described for crustacean and insect neurons (Ryglewski & Duch, 2009; Baro & Harris-Warrick, 1998; Diao et al., 2009; 2010). In MN5 action potentials are mediated by TTX sensitive fast VGSCs (Duch et al., 2008). Therefore, propagation of the action potential requires high densities of VGSCs in the axonal membrane. Across animals we found a clear increase in the density of VGSCs in the primary neurite, at a distance at about 100 microns from the soma which was always localized at ± 12 μm around the origin of the most distal dendritic sub-tree. No significant changes in sodium channel density were found along the axon

between this location and the synaptic terminals on the DLM target muscle. Although sodium channel immunopositive signal was also detected in more proximal regions of the primary neurite, at these locations the signal was distributed diffusely throughout the cytosol, thus indicating transport of sodium channel protein to the axonal domain. By contrast, at all locations more distal than 100 μm from the soma the signal was predominantly found at the edges of the primary neurite of MN5, indicating that it was in the membrane. This suggested that MN5 was specialized for active action potential propagation between this site and the target muscle. However, immunocytochemistry is not sufficient evidence to conclude unambiguously that action potentials are initiated at this location. For the following reasons we judge that this was the most likely location for action potential initiation. First, action potentials as recorded from the soma of MN5 showed amplitude attenuation and broadening. This was consistent which spike initiation at about a 100 microns distance from the soma (Duch et al., 2008). Second, an earlier study has revealed specific targeting of K_v1 Shaker potassium channels to this putative SIZ and all more distally localized parts of the axon (Ryglewski & Duch, 2009). This is consistent with K_v1 channel targeting to the axon of vertebrate neurons. Third, overexpression of VGSCs in MN5 resulted in additional localization of sodium channel to more proximal parts of the primary neurite, which in turn caused higher amplitude and sharper action potentials recorded from the soma (Ryglewski & Duch, unpublished). Therefore, we judge sodium channel immunocytochemistry as a reasonable means to detect the site of the putative action potential initiating zone in MN5. An important future challenge will be to identify scaffolding proteins that might target VGSCs and K_v1 potassium channels to the initial axonal segment of invertebrate neurons, and thus, serve as organizers for their polarization. A recent study on Drosophila mushroom body neurons has identified a function for Cdk5/p35 kinase in recruiting Ankyrin 1 to a putative initial axonal segment with molecular distinct properties (Trunova et al., 2011). This study provides the molecular tools to further verify the location of the SIZ and the initial axonal segment as a gatekeeper between the axonal and the dendritic domain of monopolar insect motoneurons in future experiments.

Evaluation of the method used for mapping putative input synapses to central dendrites of MN5 by targeted expression of tagged receptors

The distributions of putative cholinergic input was mapped onto MN5 geometric reconstructions by analyzing the localization of GFP-tagged Dα7 nAChRs expressed under the control of non-native promoters. This approach yielded a map of putative cholinergic inputs to MN5, but it also bears problems. These include the limits of light microscopy resolution, possible mis-targeting as might have been caused by false expression strength and timing, and possibly missing other alpha sub-units of the nAChR. First, the optical resolution of confocal microscopy is below the size of individual synapses. Therefore, only serial sectioning electron microscopy will yield an error free map of inputs to a central neuron (Briggman & Denk, 2006). However, despite recent advances in block face scanning EM this technique is still extremely time consuming and not at hand at most institutions. Therefore, at current a light microscopic approach seemed more reasonable. To avoid false positives resulting from labeled receptors that might have been present at non-synaptic sites we scored only those Dα7 puncta that were co-localized with MN5 dendrites and also in close proximity to the presynaptically localized active zone marker NC82. It is widely assumed that insect motoneurons contain no, or only few dendritic output synapses, indicating that co-localized NC82 puncta next to MN5 dendrites and Dα7 puncta in MN5 dendrites resemble synaptic inputs to MN5. Similarly, this approach has previously been used successfully in fly tangential neurons to detect sites of putative cholinergic (Raghu et al., 2009) and putative GABAergic synaptic inputs (Raghu et al., 2007).

However, all that can be concluded from such mapping methods is that positively scored sites are candidates for putative cholinergic input synapses, and that locations devoid of positive label do not represent input sites to the Dα7 nAChR. Accordingly, this method provides only an estimate as to whether Dα7 positive postsynaptic sites were predominantly localized to specific dendritic domains or not. Apart from that no claims on synapse density or strength can be made.

Second, expression of tagged receptors under non-endogenous promoters bears the potential problems of mis-targeting and mixing with non-tagged endogenous receptor sub-units. We carefully compared confocal image stacks following targeted expression of tagged receptors to wild-type preparations immunolabeled for Dα7 and Rdl receptors. We did not find obvious differences in receptor distribution in the neuropil regions where MN5 dendrites are located. We can't rule out that a rigorous quantification might not have shown any differences, but clearly, endogenous receptor expression showed the same obvious hot-spots of high densities that were detected following expression of tagged receptors. Similarly, the use of different GAL4 (D42-GAL4, P103.3-GAL4, C380, GAL4) drivers that express in MN5 yielded qualitatively similar results. This indicates that our data are not an artifact of over-expression or false timing of expression during development. And finally, we can't exclude the possibility to have missed cholinergic and GABAergic inputs to other receptor subunits than Dα7 and Rdl in MN5. However, Dα7 is the crucial receptor subunit for excitatory synapses to neurons in the Drosophila escape circuit (Fayyazuddin et al., 2006), expression of GFP under the control of Dα7-GAL4 selectively labels escape circuit neurons including MN1-5, and excitatory synaptic transmission to MN5 is strongly impaired in Dα7 mutants (Fayyazuddin et al., 2006). Similarly, Rdl is the most abundant sub-unit of $GABA_A$ receptors expressed in Drosophila central neurons (Harrison et al., 1996; Liu et al., 2007, Agosto et al., 2008; Raghu et al., 2007).

Taken together, we are confident that our analysis provides a valuable estimate of the rough distribution of the most abundant excitatory and inhibitory synapses to MN5 dendrites. In accordance to this, these methods have previously yielded valuable data on synapse distribution in Manduca (Duch & Mentel, 2004; Meseke et al., 2009) and Drosophila neurons (Raghu et al., 2007; 2009).

Putative excitatory cholinergic inputs to the Dα7 receptor and putative inhibitory inputs to the Rdl $GABA_A$ receptor are localized to different dendritic regions

Although all dendritic sub-trees of MN5 as well as all branch orders contained both putative cholinergic and putative GABAergic inputs, our data indicated that the highest density of putative cholinergic inputs is located to a dendritic region proximal to the soma not directly adjacent to the putative SIZ. Between different animals these regions can be occupied by different dendritic sub-trees (Vonhoff & Duch, 2010), but they are always close to the soma, distant from the putative SIZ, and receive few putative GABAergic inputs. By contrast, most GABAergic inputs are localized just anterior and in close proximity to the putative SIZ, and these regions of predominant inhibitory input are mostly devoid of excitatory cholinergic inputs. Therefore, inhibitory and excitatory inputs seem to occupy complimentary dendritic domains of MN5. This contrasts the findings in tangential neurons in the fly lobula plate where both excitatory and inhibitory inputs are targeted to the same distal dendritic domains (Raghu et al., 2007; 2009), indicating different requirements for synaptic integration in flight motoneurons and fly visual interneurons. In fact, in fly tangential neurons co-localization of excitatory and inhibitory inputs has been proposed to serve local dendritic computations, the data available on the functions of excitatory and inhibitory drive to Drosophila flight motoneurons indicate different computational requirements (see below).

Possible functional consequences of a complimentary distribution of cholinergic and GABAergic input through MN5 dendrites

Our data indicate that excitatory and inhibitory information may not be computed locally, but in separate dendritic domains of MN5. Simultaneous extracellular recordings of MN1-5 during flight have shown that all 5 motoneurons fire tonically at about every 10^{th} to 20^{th} wingbeat during flight, that their firing frequencies are increased or decreased simultaneously and rather slowly during altered wing power output demands, and that spike time precision plays no significant role for regulating asynchronous flight power muscle contractions (Levine & Wyman, 1973; Koenig & Ikeda, 1980a; b; Gordon & Dickinson, 2006). We confirmed by extracellular recordings of MN5 during restrained flight of intact animals that MN5 firing frequency remains constant at constant wing beat frequency, and that firing rate changes slowly during changes of wing beat frequency (Ryglewski & Duch, 2009; Kadas and Duch, unpublished). Although spike time precision during tonic firing is low, double spikes or sudden changes in firing frequency are not observed during constant restrained flight. Moreover, changes of motoneuron tonic firing frequency correlate linearly with changes in intramuscular calcium concentration, which, in turn, correlate linearly with changes wing beat frequency and power output over the operational range during normal restrained flight (Gordon & Dickinson, 2006). The resulting prediction has been that tonic excitatory drive is translated into different tonic firing frequencies of MN1-5 (Levine & Wyman, 1973; Harcombe & Wyman, 1977). This would not require sharp excitatory postsynaptic potentials close to the SIZ, nor would it require local dendritic computations of excitatory and inhibitory postsynaptic potentials. By contrast slow adjustments of steady tonic firing frequencies in response to increased excitatory drive can best be achieved by the summation of many EPSPs with relatively slow rise and decay times. This is consistent with a high density of excitatory inputs to dendrites that are distant to spike initiation, as found in our maps of putative cholinergic input to MN5 dendritic domains proximal to the soma.

It should be noted that all data available on motoneuron tonic firing patterns during flight derive from restrained flight preparations in which animals don't carry their own weight and maximal power output may not be required at any time. In response to current injection MN5 can fire at much higher frequencies (up to 100 Hz, Ryglewski, unpublished) than observed during restrained flight (5 to 20Hz), and MN5 following frequencies during giant fiber stimulation range up to 200 Hz (Kadas et al., 2012). Therefore, natural flight may require much higher MN5 firing frequencies. Though speculative at current, high MN5 firing frequencies during increased power demands as may be necessary during natural flight behavior may require boosting of excitatory synaptic drive by dendritic calcium channels as reported for vertebrate spinal motoneurons (Heckman et al., 2003). We know that both low and high voltage activated somatodendritic Ca_v1 and Ca_v3 calcium channels are present in MN5 (Ryglewski et al., 2012). Excitatory synaptic drive to dendritic domains distant of the SIZ could be strongly enhanced by voltage gated dendritic calcium channels, and clustering of Dα7 receptors to dendritic sub-regions would facilitate opening of dendritic calcium channels during high power demand situations. The distribution maps of dendritic Dα7 localization on MN5 are consistent with these behavioral requirements.

Inhibitory inputs are thought to not influence MN5 tonic firing frequency during flight but to affect the sequence of MN1-5 firing (Harcombe & Wyman, 1977). In contrast, simultaneous extracellular recordings of multiple DLM units during restrained flight revealed that MN5 may fire at any time during the inter-spike intervals of MN1-4, but simultaneous action potentials of MN5 and any of the other four flight motoneurons, MN1-4, occur with significantly lower likelihood. The same was found for any combination of simultaneous MN1-5 recordings, but the chance that two DLM motoneurons fired at close time point with respect to each other differed between different pairs (Harcombe & Wyman, 1977). Consequently, it was concluded that MN1-5 receive tonic excitatory drive throughout the

wing beat cycle, but inhibitory interactions within the flight motor network ensure that no motoneuron fires during the short time periods when any of the other four motoneuron fires. Different weights of inhibition between different MN1-5 pairs have been proposed to create a preferred sequence of MN1-5 firing during flight (Harcombe & Wyman, 1977). This mechanism would require fast inhibitory network interactions, because the sodium dependent action potentials of MN1-5 last only few milliseconds. This is in agreement with a high density of inhibitory inputs close to the SIZ as predicted by our anatomical Rdl receptor mapping. Sharp inhibitory postsynaptic potentials (IPSPs) are required at the spike initiating zone to prevent firing during the brief time windows when other motoneurons fire. In general, the more distal a synaptic input is located the more is PSP shape broadened (London & Haeusser, 2005). Therefore, the distribution maps of putative synaptic inputs as well as the location of the putative SIZ as inferred from our light microscopic analysis are in agreement with the existing the hypothesis that sharp inhibitory network interactions may cause a preferred sequence of MN1-5 firing during flight (Harcombe & Wyman, 1977). Furthermore, the long predicted separate functions of common tonic excitatory drive for adjusting overall firing frequencies and sharp interactions to prevent simultaneous firing indicate no need for local dendritic computations of excitatory and inhibitory synaptic drive. This is an accord with targeting most putative excitatory and inhibitory inputs to different dendritic domains. Therefore, the distribution maps for putative GABAergic and cholinergic inputs as found on the morphological level in this study support previous predictions on different functions of excitatory and inhibitory synaptic drive to Drosophila flight motoneurons during behavior which are based on extracellular recordings.

The distribution patterns for putative GABAergic inputs differ significantly between MN5 in Manduca (Meseke et al., 2009) and in Drosophila, with high densities proximal to the spike initiating zone in Drosophila but distal GABAergic synapses in Manduca. Please note that Manduca flight operates via synchronous, indirect flight muscles, where motoneuron and flight muscle fiber action potentials correlate 1:1, and high spike time precision is required in motoneurons. This strongly contrasts Drosophila asynchronous flight during which motoneuron and muscle fiber action potentials are not synchronized and motoneuron spike time precision is low. Therefore, different flight systems operate with different synapse distribution through motoneuron dendrites. Our dendritic reconstructions and putative synaptic input distribution maps can be exported to the NEURON modeling environment (Hines & Carneval, 1997; 2001) to create predictions about the possible functions of input synapse distribution through MN5 dendrites in multi-compartment models (Ryglewski & Duch, 2009; Meseke et al., 2009). Facile genetic tools available in Drosophila may help to test resulting functional hypothesis by genetic manipulation and subsequent behavioral testing.

Acknowledgments

We gratefully acknowledge support by NIH (RO1NS072128 and S10RR027154) to CD. We thank Dr. Bellen (Houston, Texas) for kindly providing the Dα7AChR antibody and Dr. Naessel (Stockholm, Sweden) for kindly providing the anti-RDL $GABA_A$ receptor antibody. We thank the Undergraduate Students Lisa Schmidtke and Nisintha Mahendrarajah (both Mainz) for help with Western blotting.

Literature

Agosto J, Choi JC, Parisky KM, Stilwell G, Rosbash M, Griffith LC. Modulation of $GABA_A$ receptor desensitization uncouples sleep onset and maintenance in Drosophila. Nat. Neurosci. 2008; 11:354–359. [PubMed: 18223647]

Amat C, Lapied B, French AS, Hue B. Sodium dependent neuritic spikes initiate calcium-dependent somatic plateau action potentials in insect dorsal paired median neurons. J. Neurophysiol. 1998; 80:2718–2726. [PubMed: 9819276]

Baines RA, Bate M. Electrophysiological development of central neurons in the Drosophila embryo. J Neurosci. 1998; 18(12):4673–4683. [PubMed: 9614242]

Baro DJ, Harris-Warrick RM. Differential expression and targeting of K+ channel genes in the lobster pyloric central pattern generator. Annu. N Y Acad. Sci. 1998; 860:281–295.

Boerner J, Puschmann T, Duch C. A steroid hormone affects sodium channel expression in Manduca central neurons. Cell Tissue Res. 2006; 325:175–187. [PubMed: 16525830]

Boerner J, Duch C. Average shape standard atlas for the adult Drosophila ventral nerve cord. J. Comp. Neurol. 2010; 518:2437–2455. [PubMed: 20503421]

Briggman KL, Denk W. Towards neural circuit reconstruction with volume electron microscopy techniques. Curr. Opin. Neurobiol. 2006; 16:562–570. [PubMed: 16962767]

Broadie K, Bate M. Development of larval muscle properties in the embryonic myotubes of Drosophila melanogaster. Neuron. 1993; 11:607–619. [PubMed: 7691105]

Consoulas C, Restifo LL, Levine RB. Dendritic remodeling and growth of motoneurons during metamorphosis of Drosophila melanogaster. J. Neurosci. 2002; 22:4906–4917. [PubMed: 12077188]

Diao F, Waro G, Tsunoda S. Fast inactivation of Shal (K(v)4) K+ channels is regulated by the novel interactor SKIP3 in Drosophila neurons. Mol. Cell. Neurosci. 2009; 42:33–44. [PubMed: 19463952]

Diao F, Chaufty J, Waro G, Tsunoda S. SIDL interacts with the dendritic targeting motif of Shal (K(v)4) K+ channels in Drosophila. Mol. Cell. Neurosci. 2010; 45:75–83. [PubMed: 20550966]

Dickinson MH, Tu MS. The function of dipteran flight muscle. Comp. Biochem. Physiol. A. 1997; 116:223–228.

Di Cristo G, Wu C, Chattopadhyaya B, Ango F, Knott G, Welker E, Svoboda K, Huang ZJ. Subcellular domain-restricted GABAergic innervation in primary visual cortex in the absence of sensory and thalamic inputs. Nat. Neurosci. 2004; 7:1184–6. [PubMed: 15475951]

Duch C, Levine RB. Remodeling of membrane properties and dendritic architecture accompanies the postembryonic conversion of a slow into a fast motoneuron. J. Neurosci. 2000; 20:6950–6961. [PubMed: 10995839]

Duch C, Bayline RJ, Levine RB. Postembryonic development of the dorsal longitudinal flight muscle and its innervation in Manduca sexta. J. Comp. Neurol. 2000; 422:1–17. [PubMed: 10842215]

Duch C, Mentel T. Activity affects dendritic shape and synapse elimination during steroid controlled dendritic retraction in Manduca sexta. J. Neurosci. 2004; 24:9826–9837. [PubMed: 15525767]

Duch C, Vonhoff F, Ryglewski S. Dendrite elongation and dendritic branching are affected separately by different forms of intrinsic motoneuron excitability. J. Neurophysiol. 2008; 100:2525–2536. [PubMed: 18715893]

Enell L, Hamasaka Y, Kolodziejczyk A, Naessel DR. γ-Aminobutyric Acid (GABA) Signaling Components in Drosophila: Immunocytochemical Localization of GABAB Receptors in Relation to the $GABA_A$ Receptor Subunit RDL and a Vesicular GABA Transporter. J. Comp. Neurol. 2007; 505:18–37. [PubMed: 17729251]

Evers JF, Schmitt S, Sibila M, Duch C. Progress in functional neuroanatomy: precise automatic geometric reconstruction of neuronal morphology from confocal image stacks. J. Neurophysiol. 2005; 93:2331–2342. [PubMed: 15537815]

Evers JF, Muench D, Duch C. Developmental relocation of presynaptic terminals along distinct types of dendritic filopodia. Dev. Biol. 2006; 297:214–227. [PubMed: 16806147]

Fayyazuddin A, Zaheer MA, Hiesinger PR, Bellen HJ. The nicotinic acetylcholine receptor Dalpha7 is required for an escape behavior in Drosophila. PLoS Biol. 2006; 4:e63. [PubMed: 16494528]

Ffrench-Constant RH, Roush RT, Mortlock D, Dively GP. Isolation of dieldrin resistance from field populations of Drosophila melanogaster (Diptera: Drosophilidae). Econ. Entomol. 1990; 83:1733–1737.

Ffrench-Constant RH, Rocheleau TA, Steichen JC, Chalmers AE. A point mutation in Drosophila GABA receptor confers insecticide resistance. Nature. 1993; 363:449–45. [PubMed: 8389005]

French AS, Sanders EJ, Duszyk E, Prasad S, Torkkeli PH, Haskins J, Murphy RA. Immunocytochemical localization of sodium channels in an insect central nervous system using a site-directed antibody. J Neurobiol. 1993; 24:939–948. [PubMed: 8228971]

Gordon S, Dickinson MH. Role of calcium in the regulation of mechanical power in insect flight. PNAS. 2006; 103:4311–4315. [PubMed: 16537527]

Grauso M, Reenan RA, Culetto E, Sattelle DB. Novel putative nicotinic acetylcholine receptor subunit genes, Dα5, Dα6 and Dα7 in Drosophila melanogaster identify a new and highly conserved target of adenosine deaminase acting on RNA-mediated A-to-I pre-mRNA editing. Genetics. 2002; 160:1519–1533. [PubMed: 11973307]

Grolleau F, Sattelle D. Single channel analysis of the blocking actions of BIDN and fipronil on a Drosophila melanogaster GABA receptor (RDL) stably expressed in a Drosophila cell line. Br. J. Pharmacol. 2000; 130:1833–1842. [PubMed: 10952672]

Harcombe ES, Wyman RJ. Output pattern generation by Drosophila flight motoneurons. J. Neurophysiol. 1977; 40:1066–77. [PubMed: 409808]

Harrison JB, Chen HH, Sattelle E, Barker PJ, Huskisson NS, Rauh JJ, Bai D, Sattelle DB. Immunocytochemical mapping of a C-terminus anti-peptide antibody to the GABA receptor subunit, RDL in the nervous system in Drosophila melanogaster. Cell Tissue Res. 1996; 284:269–278. [PubMed: 8625394]

Häusser M, Mel B. Dendrites: bug or feature? Curr. Opin. Neurobiol. 2003; 13(3):372–383. [PubMed: 12850223]

Heckman CJ, Lee RH, Brownstone RM. Hyperexcitable dendrites in motoneurons and their neuromodulatory control during motor behavior. Trends Neurosci. 2003; 26:688–695. [PubMed: 14624854]

Hedstrom KL, Xu X, Ogawa Y, Frischknecht R, Seidenbecher CI, Shrager P, Rasband MN. Neurofascin assembles a specialized extracellular matrix at the axon initial segment. J. Cell Biol. 2007; 178:875–886. [PubMed: 17709431]

Hill AS, Nishino A, Nakajo K, Zhang G, Fineman JR, Selzer ME, Okamura Y, Cooper EC. Ion channel clustering at the axon initial segment and node of Ranvier evolved sequentially in early chordates. PLoS Genet. 2008; 4:e1000317. [PubMed: 19112491]

Hines ML, Carnevale NT. The NEURON simulation environment. Neural Comput. 1997; 9:1179–1209. Review. [PubMed: 9248061]

Hines ML, Carnevale NT. NEURON: a tool for neuroscientists. Neuroscientist. 2001; 7:123–135. Review. [PubMed: 11496923]

Hohensee S, Bleiss W, Duch C. Correlative electron and confocal microscopy assessment of synapse localization in the central nervous system of an insect. J. Neurosci. Methods. 2008; 168:64–70. [PubMed: 17980437]

Ikeda K, Koenig JH. Morphological identification of the motor neurons innervating the dorsal longitudinal flight-muscle of Drosophila melanogaster. J. Comp. Neurol. 1988; 273:436–444. [PubMed: 3145293]

Ishizuka N, Weber J, Amaral DG. Organization of intrahippocampal projections originating from CA3 pyramidal cells in the rat. J. Comp. Neurol. 1990; 295:580–623. [PubMed: 2358523]

Kadas D, Tzortzopoulos A, Skoulakis EM, Consoulas C. Constitutive activation of Ca2+/calmodulin-dependent protein kinase II during development impairs central cholinergic transmission in a circuit underlying escape behavior in Drosophila. J. Neurosci. 2012; 32:170–82. [PubMed: 22219280]

Katz Y, Menon V, Nicholson DA, Geinisman Y, Kath WL, Spruston N. Synapse distribution suggests a two-stage model of dendritic integration in CA1 pyramidal neurons. Neuron. 2009; 63:171–7. [PubMed: 19640476]

Koch C, Segev I. The role of single neurons in information processing. Nat. Neurosci. 2000; (Suppl.): 1171–1177. [PubMed: 11127834]

Koenig JH, Ikeda K. Neural interactions controlling timing of flight muscle activity in Drosophila. J. Exp. Biol. 1980a; 87:121–136. [PubMed: 7420011]

Koenig JH, Ikeda K. Interspike interval relationship among flight muscle fibres in Drosophila. J. Exp. Biol. 1980b; 87:137–147. [PubMed: 6775035]

Leech CA, Sattelle DB. Acetylcholine receptor/channel molecules of insects. EXS. 1993; 63:81–97. [PubMed: 7678532]

Levine JD, Wyman RJ. Neurophysiology of flight in wild-type and a mutant Drosophila. PNAS. 1973; 70:1050–1054. [PubMed: 4197927]

Li XG, Somogyi P, Ylinen A, Buzsáki G. The hippocampal CA3 network: an in vivo intracellular labeling study. J. Comp. Neurol. 1994; 339:181–208. [PubMed: 8300905]

Liu X, Krause WC, Davis RL. $GABA_A$ receptor RDL inhibits Drosophila olfactory associative learning. Neuron. 2007; 56:1090–1102. [PubMed: 18093529]

London M, Häusser M. Dendritic computation. Ann. Rev. Neurosci. 2005; 28:503–532. [PubMed: 16033324]

Machin KE, Pringle JWS. The physiology of insect fibrillar muscle. II. Mechanical properties of a beetle flight muscle. Proc. R. Soc. Lond. 1959; 151B:204–225.

Mee CJ, Pym EC, Moffat KG, Baines RA. Regulation of neuronal excitability through pumilio-dependent control of a sodium channel gene. J. Neurosci. 2004; 24:8695–86703. [PubMed: 15470135]

Meseke M, Evers JF, Duch C. Developmental changes in dendritic shape and synapse location tune single-neuron computations to changing behavioral functions. J. Neurophysiol. 2009; 102:41–58. [PubMed: 19386754]

Pan Z, Kao T, Horvath Z, Lemos J, Sul JY, Cranstoun SD, Bennett V, Scherer SS, Cooper EC. A common ankyrin-G-based mechanism retains KCNQ and NaV channels at electrically active domains of the axon. J. Neurosci. 2006; 26:2599–2613. [PubMed: 16525039]

Pouille F, Scanziani M. Enforcement of temporal fidelity in pyramidal cells by somatic feed-forward inhibition. Science. 2001; 293:1159–1163. [PubMed: 11498596]

Raghu SV, Joesch M, Borst A, Reiff D. Synaptic organization of lobula plate tangetntial cells in Drosophila: gamma-aminobutyric acid receptors and chemical release sites. J. Comp. Neurol. 2007; 502:598–610. [PubMed: 17394161]

Raghu SV, Joesch M, Sigrist SJ, Borst A, Reiff DF. Synaptic organization of lobula plate tangential cells in Drosophila: Dalpha7 cholinergic receptors. J. Neurogenet. 2009; 23:200–209. [PubMed: 19306209]

Ransband MN. The axon initial segment and the maintenance of neuronal polarity. Nat. Rev. Neurosci. 2010; 11:552–562. [PubMed: 20631711]

Ryglewski S, Duch C. Shaker and Shal mediate transient calcium-independent potassium current in a Drosophila flight motoneuron. J. Neurophysiol. 2009; 102:3673–3688. [PubMed: 19828724]

Ryglewski S, Lance K, Levine R, Duch C. Cav2 channels mediate LVA and HVA calcium currents in Drosophila motoneurons. J. Physiol. 2012; 590:809–825. [PubMed: 22183725]

Sánchez-Soriano N, Bottenberg W, Fiala A, Haessler U, Kerassoviti A, Knust E, Löhr R, Prokop A. Are dendrites in Drosophila homologous to vertebrate dendrites? Dev. Biol. 2005; 288:126–138. [PubMed: 16223476]

Sanyal S, Narayanan R, Consoulas C, Ramaswami M. Evidence for cell autonomous AP1 function in regulation of Drosophila motor-neuron plasticity. BMC Neurosci. 2003; 11:4:20.

Sanyal S. Genomic mapping and expression patterns of C380, OK6 and D42 enhancer trap lines in the larval nervous system of Drosophila. Gene Expr. Patterns. 2009; 9:371–380. [PubMed: 19602393]

Schmitt S, Evers JF, Duch C, Scholz M, Obermayer K. New methods for the computer-assisted 3-D reconstruction of neurons from confocal image stacks. Neuroimage. 2004; 23:1283–1298. [PubMed: 15589093]

Somogyi P, Tamás G, Lujan R, Buhl EH. Salient features of synaptic organisation in the cerebral cortex. Brain Res. Rev. 1998; 26:113–135. [PubMed: 9651498]

Stricker C, Field AC, Redman SJ. Statistical analysis of amplitude fluctuations in EPSCs evoked in rat CA1 pyramidal neurones in vitro. J. Physiol. 1996; 490:419–441. [PubMed: 8821140]

Su H, O'Dowd DK. Fast synaptic currents in drosophila mushroom body kenyon cells are mediated by alpha-bungarotoxin-sensitive nicotinic acetylcholine receptors and picrotoxin-sensitive gaba receptors. J. Neurosci. 2003; 23:9246–9253. [PubMed: 14534259]

Trunova S, Baek B, Giniger E. Cdk5 regulates the size and axon initial segment-like compartment in mushrrom body neurons of the Drosophila central brain. J. Neurosci. 2011; 31:10451–10462. [PubMed: 21775591]

Van Wart A, Trimmer JS, Matthews G. Polarized distribution of ion channels within microdomains of the axon initial segment. J. Comp. Neurol. 2007; 500:339–352. [PubMed: 17111377]

Vonhoff F, Duch C. Tiling among stereotyped dendritic branches in an identified Drosophila motoneuron. J. Comp. Neurol. 2010; 518:2437–2455. [PubMed: 20503421]

Wagh DA, Rasse TM, Asan E, Hofbauer A, Schwenkert I, Duerrbeck H, Buchner S, Dabauvalle MC, Schmidt M, Qin G, Wichmann C, Kittel R, Sigrist SJ, Buchner E. Bruchpilot, a protein with homology to ELKS/CAST, is required for structural integrity and function of synaptic active zones in Drosophila. Neuron. 2006; 49:833–844. [PubMed: 16543132]

Yeh E, Gustafson K, Boulianne GL. Green fluorescent protein as a vital marker and reporter of gene expression in Drosophila. PNAS. 1995; 92:7036–7049. [PubMed: 7624365]

Zhou D, Lambert S, Malen PL, Carpenter S, Boland LM, Bennett V. AnkyrinG is required for clustering of voltage-gated Na channels at axon initial segments and for normal action potential firing. J. Cell Biol. 1998; 143:1295–130. [PubMed: 9832557]

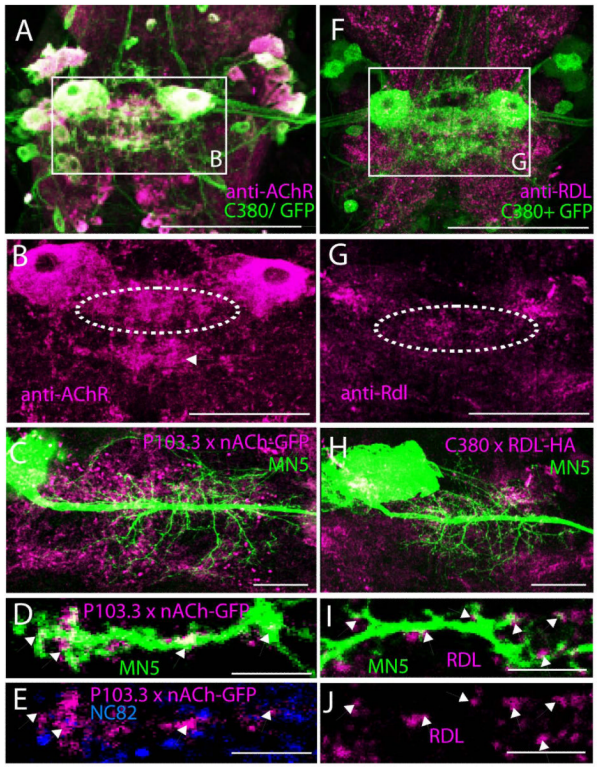

Figure 1. Dα7 nAChR and Rdl $GABA_A$ receptor localization in the adult flight motor neuropil

(A) Double label immunohistochemistry for Dα7 nAChRs (magenta) and GFP (green) in the ventral nerve cord of animals expressing UAS-GFP under the control of the motoneuron driver C380-GAL4; Cha-GAL80. Co-localization appears white. White rectangle demarks both left and right MN5. (B) Selective enlargement of Dα7 nAChRs immunolabel from white rectangle in A. MN5 somata are Dα7 positive, and punctuated Dα7 label is found throughout the neuropil region that contains MN5 dendrites (dotted white oval). However, dense punctuated Dα7 label is also present outside the dendritic region of flight motoneurons (white arrow). (C) Intracellular staining of MN5 (green) superimposed on Dα7-GFP label (magenta) in a representative animal with UAS-Dα7-GFP expressed under the control of the motoneuron driver P103.3-GAL4. Punctuated Dα7 label in neuropil appears similar following overexpression of GFP tagged Dα7 receptors (C) and following immunohistochemistry for native Dα7 protein in the flight motor neuropil (B). (D) Selective enlargement of a single optical section containing one MN5 dendritic branch (green) and Dα7-GFP puncta (magenta). Overlap of MN5 dendrite staining and Dα7-GFP puncta appear white and are demarked by arrows. (E) Same optical section as in (D) but shown are only anti-Dα7-GFP puncta and anti-NC82 puncta (presynaptic marker). Dα7-GFP puncta that were co-localized with MN5 dendrite as shown in (D) are directly adjacent to NC82 positive presynaptic terminals. (F) Double label immunohistochemistry for Rdl $GABA_A$ receptors (magenta) and GFP (green) in the ventral nerve cord of animals expressing UAS-GFP under the control of the motoneuron driver C380-GAL4; Cha-GAL80. Co-localization appears white. White rectangle demarks both left and right MN5. (G) Selective enlargement of Rdl $GABA_A$ receptor immunolabel from white rectangle in A. Punctuated Rdl label is found throughout the neuropil region that contains MN5 dendrites (dotted white oval), but also present in other neuropil regions. (H) Intracellular staining of MN5 (green) superimposed on Rdl-HA label (magenta) in a representative animal with UAS-Rdl-HA expressed under the control of the motoneuron driver C380-GAL4; Cha-GAL80. Punctuated Rdl label in neuropil appears similar following overexpression of HA tagged Rdl receptors

(H) and following immunohistochemistry for native Rdl protein in the flight motor neuropil (G). (I) Selective enlargement of a single optical section containing one MN5 dendritic branch (green) and Rdl-HA puncta (magenta). Overlap of MN5 dendrite staining and Rdl-HA puncta appear white and are demarked by arrows. (J) Same optical section as in (I) but shown are only anti-Rdl-HA puncta. Scale bars: 150 μm in A and F, 100 μm in B and G, 50 μm in C and H, and 2 μm in D, E, I, and J.

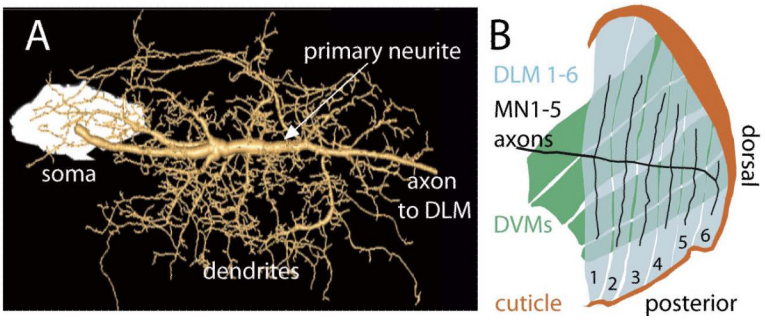

Figure 2. MN5 and the dorsal longitudinal flight muscle

(A) Geometric MN5 dendrite reconstruction superimposed on a projection view of intracellular dye fill. The soma of MN5 is to the left (white). Soma and axon are connected by a prominent primary neurite (see white arrow), which gives rise to all dendrites. (B) Schematic drawing of inner view of the six fibers of the dorsal longitudinal flight muscle (DLM, blue) and its innervation by the flight motoneurons, MN1-5 (black). MN1-4 each innervate one of the four the ventral most DLM fibers, and MN5 innervates the two dorsal most DLM fibers. More external dorso-ventral flight muscles (DVMs) are shown in green, and the dorsal cuticle is shown in brown.

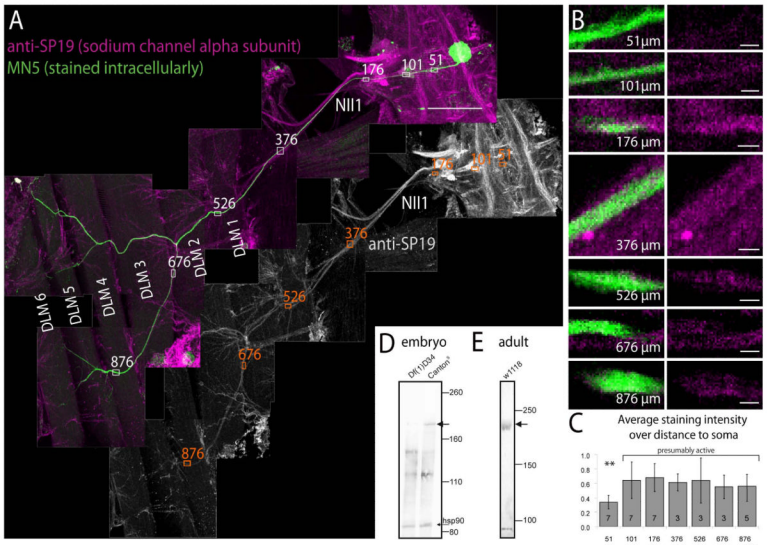

Figure 3. Localization of voltage gated sodium channels in the ventral nerve cord and in MN5

(A) Immunohistochemistry for voltage gated sodium channels (VGSCs; magenta, upper panel; grey scale lower panel) paired with intracellular staining of MN5 (green). Several fields of view are shown as one montage that contains the pterothoracic part of the CNS, nerve NII1 to the dorsal longitudinal flight muscle (DLM), and the six fibers of the DLM (labeled DLM1-6). Within the CNS prominent axon fascicles in tracts and commissures are immunopositive for VGSCs. MN5 (green) is labeled by somatic dye injection, and its axon can be followed all the way to the two dorsal most DLM fibers (DLM5 and DLM6). Axons in nerve NII1 are immunopositive for VGSCs (see grey channel for VGSC immunostaining). Small white rectangles with numbers mark the axon of MN5 at different distances from its soma (51 μm is within the primary neurite, 101 μm is at the origin of the most distal first order dendrite, 376 μm is in nerve NII1 proximal to the DLM, 526 μm is where the NII1 reaches the DLM, and 876 μm is at just before MN5 axon branches of DLM fibers 5 and 6). (B) At each of these distances, representative single sections of MN5 and VGSC label are selectively enlarged (left column double labels, right column sodium channel immunolabel only). At 51 μm distance only faint immunopositive label for VGSCs is found in the axon of MN5 (first row). At 101 μm distance from the soma immunolabel for VGSCs in MN5 axon is stronger (second row). At all more distal locations within nerve II1A strong immunolabel for VGSCs is detected. (C) Quantification of VGSC immunostaining intensities at the distances shown in B over multiple animals (number of samples in each bar). Data were normalized to highest intensity signal in each preparation. No significant differences in VGSC immunopositive signal intensities are detected along MN5 axon between the origin of the most distal dendrite in the CNS (101 μm from MN5 soma) and the target muscle fibers DLM5-6 (ANOVA, $p \geq 0.3$). By contrast more proximal parts of the MN5 primary neurite (e.g. 51 μm from the soma) show significantly lower staining intensities for VGSCs (ANOVA with Newman Keuls post hoc test, $p \leq 0.01$). Scale bars: 100 μm in A, 3 μm in B. (D) Western blot from stage 16 wild type embryos (right lane) reveals a band at the size expected for Drosophila VGSC α-subunit(para, predicted size 230 kDa, see black arrow). This band is not present in stage matched para mutant embryos (Df(1)D34, left lane), see black arrow). Protein loading was similar as revealed by similarly strong bands for heat shock protein 90 (hsp90) on both lanes (see black arrow). (E) Western blot against adult brain homogenate confirms that the SP19 antibody recognized a protein of the size predicted for Drosophila VGSC α-subunit (para, predicted size 230 kDa, see black arrow).

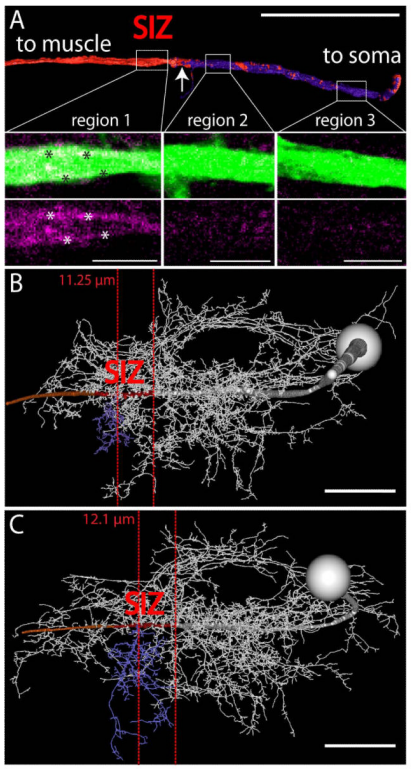

Figure 4. Estimating the location of the putative spike initiating zone of MN5

(A) shows a surface reconstruction of MN5 primary neurite. MN5 soma is to the right and the axon is to the left. White rectangles demark three regions for which single optical sections of original MN5 staining and immunocytochemistry data for VGSCs are shown as selective enlargements in lower panels. Regions 3 (right) and 2 (middle) show faint immunopositive signal for VGSCs evenly distributed through the primary neurite of MN5. Region 1 (left) shows higher intensity immunolabel for VGSCs in MN5 primary neurite, and most of this signal seems to be confined to the membrane of MN5 primary neurite (white asterisks). VGSC staining intensities are depicted as heat map (low intensities are dark blue and high ones are red) on the surface reconstruction of the MN5 primary neurite. A sharp border between low and high staining intensities for VGSCs is found at about 100 μm from the soma of MN5. (B, C) Same procedure as in (A) for two complete geometric reconstructions of MN5. Primary neurite regions with high labeling intensities for VGSCs are in red, most distal posterior dendrite originating from MN5 primary neurite is in blue. In (B) the sharp border between low and high labeling intensities for VGSCs is located 11.25 μm around the origin of the blue dendrite, and in (C) it is located 12.1 μm around the origin of the blue dendrite. Scale bars: 4 μm in A, 50 μm in B and C.

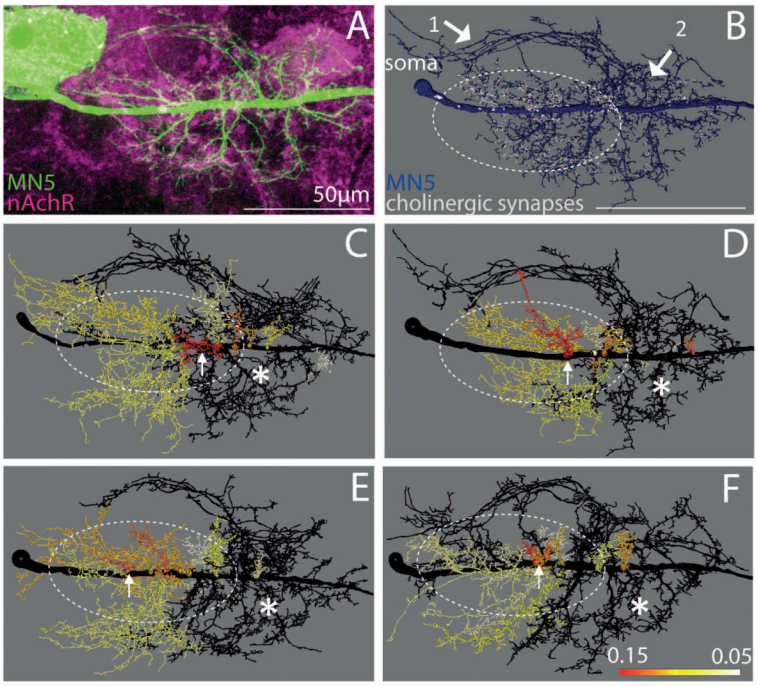

Figure 5. Distribution of putative cholinergic inputs to the Dα7 nAChR through MN5 dendrites

(A) Representative projection view of intracellular staining of MN5 (green) and GFP-tagged *Dα7* receptors following expression of Dα7-GFP under the control of P103.3-GAL4. (B) Mapping of Dα7-GFP puncta (white) that are co-localized with MN5 dendrites and within 300 nm of NC82 puncta (see methods) onto the surface reconstruction of MN5 (blue). (C to F) Heat color map ranks all dendritic sub-trees that contain 75% of all putative cholinergic inputs to MN5. Dotted white oval demarks area that contains ≥ 75 % of all positively scored Dα7-GFP puncta. All black dendrites together receive less than 25 % of all cholinergic inputs. Sub-trees with higher proportions of cholinergic inputs were color coded according to their proportion of putative cholinergic inputs (red sub-tree receives 15 % of all cholinergic inputs, orange 11%, yellow 7%, white < 5%). White arrow demarks dendritic sub-tree (red) with highest density of putative cholinergic inputs. White asterisks demark region mostly devoid of any Dα7-GFP puncta. Scale bar: 70 µm.

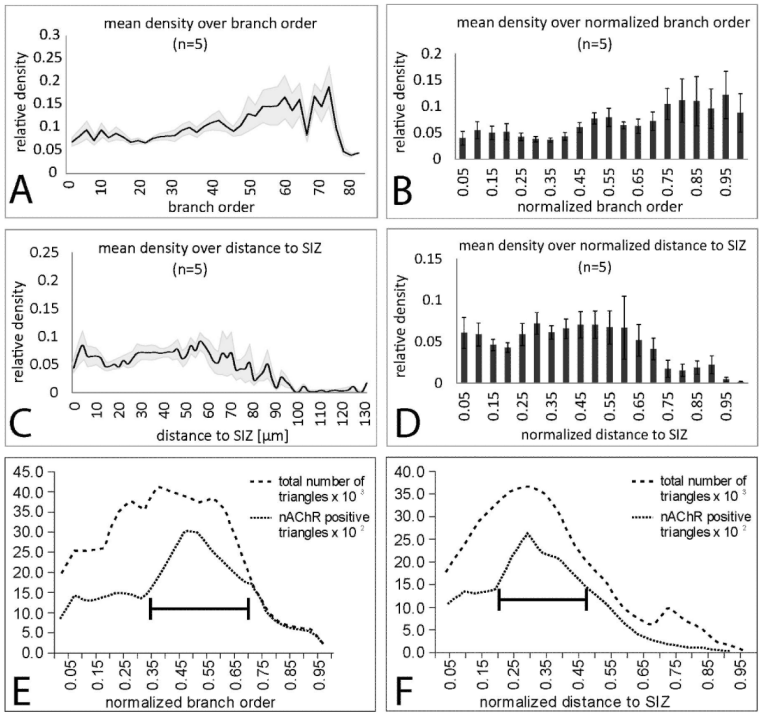

Figure 6. Quantification of distribution of putative cholinergic inputs through MN5 dendrites

(A) Mean density (black line) and standard error (gray shaded area) of positively scored Dα7-GFP puncta on MN5 dendrites over branch order. For branch order definition the putative SIZ was defined as tree origin. (B) Mean density of positively scored Dα7-GFP puncta on MN5 dendrites over normalized branch order. Normalization was done with respect to highest order branch in each animal. (C) Mean density (black line) and standard error (gray shaded area) of positively scored Dα7-GFP puncta on MN5 dendrites over absolute dendritic distance from the putative SIZ. (D) Mean density of positively scored Dα7-GFP puncta on MN5 dendrites over normalized dendritic distance to putative SIZ. Normalization was conducted relative to the largest distance present in each reconstruction. (E) Total numbers of dendritic surface triangles (dashed line) and dendritic surface triangles that were scored positive for putative cholinergic input over normalized branch order. Black bar demarks normalized branch orders with highest area of positively scored dendritic surface. (F) Total numbers of dendritic surface triangles (dashed line) and dendritic surface triangles that were scored positive for putative cholinergic input over normalized dendritic distance to the spike initiating zone. Black bar demarks normalized distances with highest area of positively scored surface dendritic.

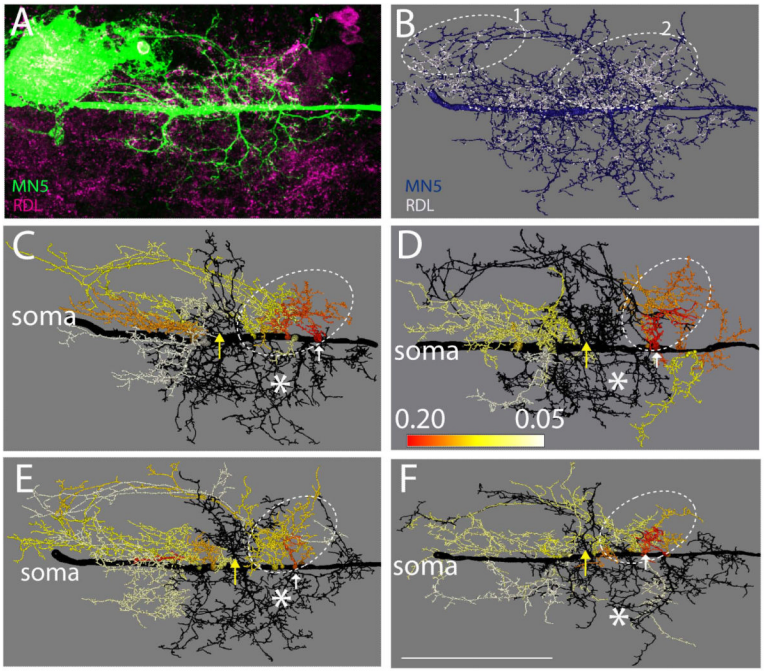

Figure 7. Distribution of putative GABAergic inputs to Rdl receptors through MN5 dendrites

(A) Representative projection view of intracellular staining of MN5 (green) and HA-tagged Rdl receptors (magenta) following expression of Rdl-HA under the control of C380-GAL4; Cha-GAL80. (B) Mapping of positively scored Rdl-HA puncta (white) onto the surface reconstruction of MN5 (blue). (C to F) Heat color map ranks all dendritic sub-trees that contain 75% of all putative GABAergic inputs to MN5. Dotted white oval demarks area that contains the highest density of all positively scored Rdl-HA puncta. All black dendrites together receive less than 25 % of all putative GABAergic inputs. Sub-trees with higher proportions of inputs were color coded according to their how many percent of all putative GABAergic inputs they received (red sub-tree, 20 %, orange 16%, yellow 12%, white < 5%). White arrow demarks dendritic sub-tree (red) with highest proportion of putative cholinergic inputs. White asterisks demark region mostly devoid of any Dα7-GFP puncta. Scale bar: 70 μm. White arrows demark root of dendritic sub-tree with highest densities of Rdl-HA puncta. White asterisks demark region mostly devoid of any Rdl-HA puncta. Scale bar: 70 μm for A to F.

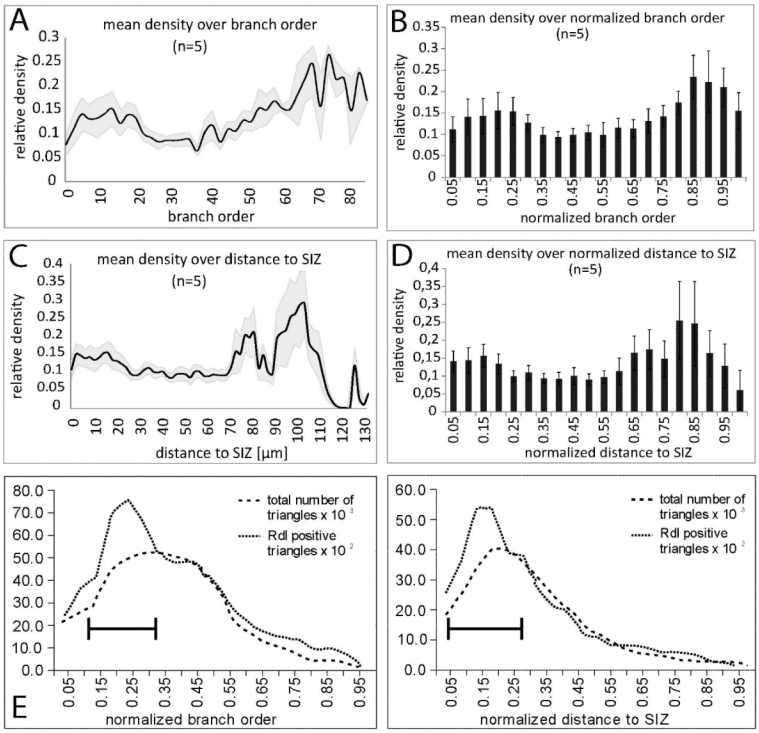

Figure 8. Quantification of distribution of putative GABAergic inputs through MN5 dendrites

(A) Mean density (black line) and standard error (gray shaded area) of positively scored positively scored Rdl-HA puncta on MN5 dendrites over branch. For branch order definition the putative SIZ was defined as tree origin. (B) Mean density of positively scored Rdl-HA puncta on MN5 dendrites over normalized branch order. Normalization was done with respect to highest order branch in each animal. (C) Mean density (black line) and standard error (gray shaded area) of positively scored Rdl-HA puncta on MN5 dendrites over absolute dendritic distance from the putative SIZ. (D) Mean density of positively Rdl-HA puncta on MN5 dendrites over normalized dendritic distance to putative SIZ. Normalization was conducted relative to the largest distance present in each reconstruction. (E) Total numbers of dendritic surface triangles (dashed line) and dendritic surface triangles that were scored positive for putative GABAergic input (dotted line) over normalized branch order. Black bar demarks normalized branch orders with highest area of positively scored dendritic surface. (F) Total numbers of dendritic surface triangles (dashed line) and dendritic surface triangles that were scored positive for putative GABAergic input (dotted line) over normalized dendritic distance to the spike initiating zone. Black bar demarks normalized distances with highest area of positively scored surface dendritic.

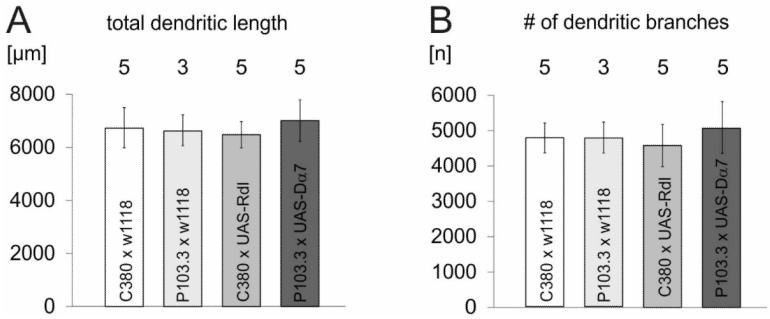

Figure 9. Total dendritic length and the number of branches are not affected by targeted expression of tagged receptors

(A) Total dendritic length of MN5 in controls for the C380-GAL4 background (C380-GAL4 × w1118, white bar, n = 5), in controls for the P103.3-GAL4 background (P103.3-GAL4 × w1118, light grey bar, n = 3), following overexpression of UAS-Rdl-HA under the control of C380-GAL4, Cha-GAL80 (grey bar, n = 5), and following overexpression of UAS-Dα7-GFP under the control of P103.3-GAL4, Cha-GAL80 (dark grey bar, n = 5). (B) Numbers of MN5 dendritic branches for the corresponding four genotypes. Bars are averages and error bars demark standard deviation. No statistical differences were found between any of the groups (ANOVA).